AD-A078 574 AIR FORCE CAMBRIDGE RESEARCH LABS HANSCOM AFB MA F/G 18/3
OPERATION SNAPPER, NEVADA PROVING GROUNDS, APRIL-JUNE 1952. PRO--ETC(U)
FEB 53 N A HASKELL , J O VANN

UNCLASSIFIED AEC-WT-511 NL

1 OF 1
AD-
A078574

END
DATE
FILMED
1-80
DDC

[redacted] UNCLASSIFIED

This document consists of 59 pages
No. 220 of 306 copies, Series A

OPERATION SNAPPER

Project 1.1

THE MEASUREMENT OF FREE AIR ATOMIC BLAST PRESSURES

REPORT TO THE TEST DIRECTOR

by

NORMAN A. HASKELL

and

JAMES O. VANN
Lt. Col., U. S. Air Force

February 1953

Terrestrial Sciences Laboratory
Geophysics Research Directorate
Air Force Cambridge Research Center

[redacted] [redacted]

UNCLASSIFIED

Reproduced Direct from Manuscript Copy by
AEC Technical Information Service
Oak Ridge, Tennessee

Inquiries relative to this report may be made to

Chief, Armed Forces Special Weapons Project
P. O. Box 2610
Washington, D. C.

If this report is no longer needed, return to

AEC Technical Information Service
P. O. Box 401
Oak Ridge, Tennessee

[redacted]

ABSTRACT

Shock overpressure as a function of time has been measured by utilizing an array of parachute-borne pressure gages spread over a wide range of distances and altitudes above two atomic detonations. The operation was accomplished by deploying 16 parachute-borne canisters from two aircraft at each shot. Each canister contained an altimeter transducer, two differential pressure transducers, a radio telemetry transmitter, and a radio tracking beacon. The telemetered pressure data were recorded at a ground station and the position of each canister was determined by radio range measurements from three multiple object tracking stations. The dropping aircraft were guided to a predetermined drop point with reference to both position and time by two SCR 584 radar stations.

The observed peak overpressures, covering the range from about 0.1 to 3.0 psi., confirm existing theory on the effect of altitude on shock overpressure to within practical accuracy requirements, and supplement other free-air peak overpressure measurements made at higher overpressures by other methods.

It is recommended that additional measurements of this kind be made at an air burst atomic test to obtain information on true free air peak overpressures, reflected shock overpressures, and the path of the Mach triple point, which could not be obtained from the present tests because of the low height of burst.

[redacted]

CONTENTS

ILLUSTRATIONS

TABLES

CHAPTER 1

INTRODUCTION

1.1 OBJECTIVE

The primary objective of the project was to measure the free air peak blast overpressure of an atomic detonation over a wide range of altitudes and distances to test the Fuchs scaling law for altitude effects. Secondary objectives were to test operational procedures and instrumentation to improve techniques and increase accuracy of measurements for a later operation involving an air burst atomic detonation.

1.2 HISTORICAL

The military requirements for an experimental test of the Fuchs theory were brought to the attention of the Terrestrial Sciences Laboratory, early in 1950. At that time a proposal was prepared for participation in Operation GREENHOUSE. However, time factors for preparation and logistics of such an extensive project were insufficient and no action was taken.

In December, 1950, the proposal was reinstated under Operation WINDSTORM and the project was officially included in February, 1951. After Operation WINDSTORM was cancelled, the project was tentatively included in Operation BUSTER but due to unsuitable frequency requirements the project was diverted to Operation JANGLE on a reduced operational scale.

The operational procedure in JANGLE consisted of deployment of eight pressure instrumented parachute-borne canisters from two aircraft. Conclusions from this operation [1] were considered tentative since the positions actually attained by the parachute-borne canisters were inconsistent with the intended vertical array and did not provide a clear cut test of the Fuchs altitude correction. There was justification, however, for concluding that the data obtained supported the Fuchs theory within the probable accuracy of the observations out to overpressures of about 0.1 psi.

---

[1] N. A. Haskell, J. O. Vann, The Measurement of Free Air Atomic Blast Pressures, Armed Forces Special Weapons Project, Operation JANGLE, Project 1.3c, Air Force Cambridge Research Center.

PRECEDING PAGE BLANK-NOT FILMED

CHAPTER 2

EXPERIMENTAL PROCEDURES

2.1 INSTRUMENTATION

The instrumentation involved in Operation SNAPPER was designed to accomplish four objectives: (1) radio telemetry instrumentation to obtain free air pressure data, (2) canister tracking instrumentation to obtain time-space data of the parachute-borne canisters, (3) radar instrumentation to position the aircraft for deployment of 16 canisters in the environs above the atomic detonation, and (4) the parachute-borne canister instrumentation to suspend probes and electronic equipment in the blast field.

Reference is made to Operation JANGLE Report, Project 1.3c, for a detailed description of the basic design of the radio telemetry system, canister tracking system and canister instrumentation.

2.1.1 Radio Telemetry Instrumentation

Each parachute-borne canister contained a pressure altimeter transducer, two differential pressure transducers (one having a scale ratio of approximately 2 with respect to the other) and a radio telemetry transmitting unit. Pressure stimulus caused each transducer in the canister to frequency modulate a sub-carrier; the three sub-carriers were mixed and subsequently frequency modulated the radio frequency carrier, the data link between the canister and the recording ground station. The recording ground station was instrumented with a separate FM receiver for each parachute-borne canister. The output of each receiver, a mixture of the three frequency modulated sub-carriers, was separated by filter networks. Subsequently each sub-carrier was channeled to a discriminator which produced an electrical current proportional to the original pressure. These proportional currents were applied to galvanometers of the recording oscillograph.

The radio telemetry system, pressure measuring instrumentation, and parachute-borne canister were developed and fabricated by the Pacific Division Development Laboratory, Bendix Aviation Corporation, Burbank, California, under Contract AF 19(122)-459.

2.1.2 Canister Tracking System

The Multiple Object Tracking (MOTS) System was used to determine the time-space data of the parachute-borne canisters. The system is based on triangulation by obtaining radio range measurements

from the canisters in space to three ground interrogating stations. The system has been designed for tracking 32 objects in space with an accuracy of approximately 100 feet.

All ground stations shared time during each second to alternately interrogate each parachute-borne canister for range data. Interrogation was accomplished by transmitting from the ground station a binary code train of five digits and a range pulse which simultaneously initiated the operation of the range counting circuit. Each airborne beacon in the canister was designed for a selected binary pulse train which was established in each beacon decoder. The decoder differentiated between the selected pulse train and all others so as to modulate the responder only when the selected pulse train was received. After this series of events the responder initiated a single reply pulse. When received by the ground station, this reply pulse stopped the range circuit counter and recorded the range count in increments of 0.1 micro-seconds, equivalent to 50 feet in range. The recorded time interval established the range from the ground station to the parachute-borne canister. A separate time mark on the recording tape established the referenced time of the canister position to standard time.

2.1.3 Aircraft Positioning Instrumentation

The two B-29 aircraft were guided over a drop point, both in reference to time and course, by using two SCR 584 radar tracking stations. Sixteen parachute-borne canisters were deployed, eight from each B-29 aircraft, at a computed drop time and drop position, corrected for the integrated horizontal wind drift of the canister.

2.1.4 Canister Instrumentation

The electronic instrumentation in the canister has been described above. The dual parachute system consisted of two parachutes, a 6-foot fist ribbon parachute and a 28-foot square semi-ribbon parachute. The latter parachute was designed for this test at WADC for the specific purpose of minimizing parachute oscillation during descent. As each canister was deployed from the aircraft the 6-foot ribbon parachute was immediately opened by the attached static line. Canister ballistic data and the particular canister position in the array determined the time of canister fall with the 6-foot ribbon parachute. At a pre-determined time, different for each canister, an internal timer fired a squib which tripped a cutter mechanism which in turn detached the 6-foot ribbon parachute, released the 28-foot square parachute. The

parechute-borne canister complete with dual parachutes weighed 275 pounds and was 86.25 inches over-all length, and 14 inches in diameter.

2.2 CALIBRATION PROCEDURE

Reference is made to Operation JANGLE Report, Project 1.3c for a detailed description of calibration procedures.

2.3 OPERATIONS SHOT 5

The problems of the operation consisted of five phases: (1) the guidance of two B-29 aircraft over a drop point both in reference to position and time (two SCR 584 radar tracking units assisted in this operation); (2) the determination of the integrated horizontal drift of the parachute-borne canisters in the wind structure in order to determine a corrected drop point for the aircraft; (3) the deployment of eight parachute-borne canisters from each of two B-29 aircraft; (4) the tracking of the 16 canisters with the Multiple Object Tracking System; and (5) the recording of telemetered blast pressure profiles from each canister.

The location of the radio telemetry station, the MOTS stations and the SCR 584 radar station are indicated in Figure 2.1.

2.3.1 Low Aircraft Operation

The low aircraft operated at 24,400 feet MSL at a true ground speed of 300 feet per second. The expected speed of 350 feet per second could not be attained because of high winds. Six practice runs were made between H-3 hours and H-30 minutes. For purposes of checking drift which was previously calculated from meteorological data, two canisters were deployed, one at H-2½ hours and one at H-1½ hours. At time of deployment, interrogation signals from both canisters failed to reach the MOTS stations. The cause of this failure is not known. Because of a malfunction in the bomb release mechanism, No. 9 canister was deployed in the place of the second drift measurement canister. In the operational run the plane was 5 seconds ahead of schedule resulting in a positional error of 1500 feet. The canisters were deployed at the scheduled time regardless of position. Deployment of canisters for the array positions Nos. 9 through 16 was initiated at H-178 seconds and completed at H-76 seconds. The positions of the canisters at shock wave arrival time are compared with the intended position in Figure 2.2.

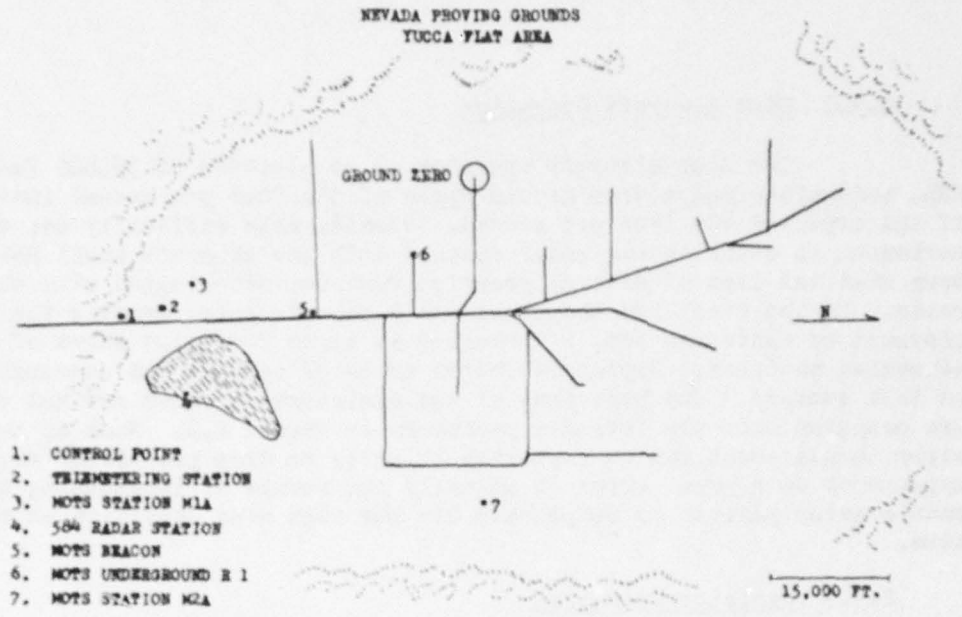

Fig. 2.1 Station Locations for Shot 5

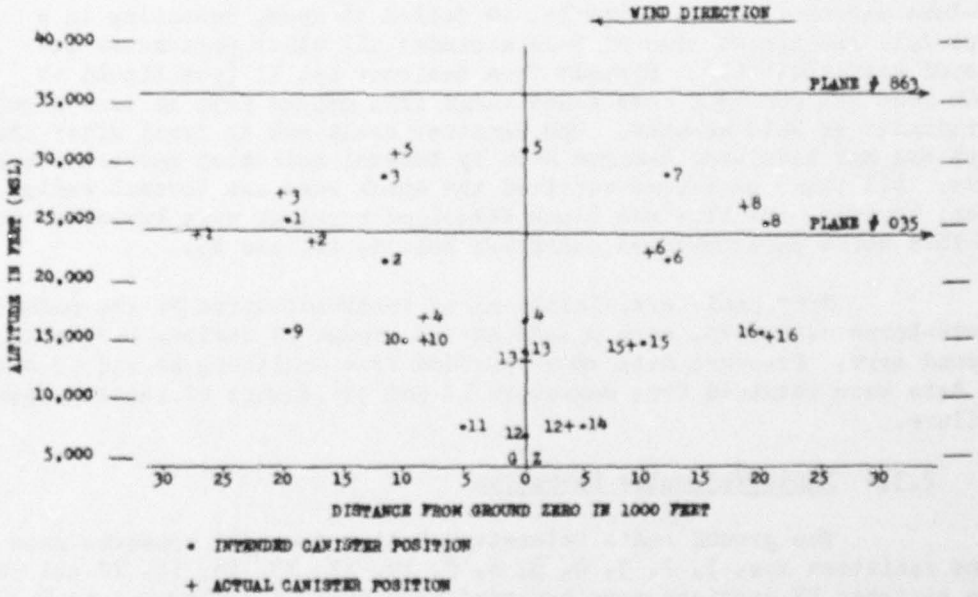

Fig. 2.2 Canister Array for Shot 5

2.3.2 High Aircraft Operation

The high aircraft operated at an altitude of 35,800 feet MSL, and maintained a true ground speed of 317 feet per second instead of the expected 400 feet per second. Considerable difficulty was experienced in establishing radar contact with the aircraft until H-1 hour when the last of several practice runs was coordinated with the radar. In the final run the plane was 9 seconds late, causing the deployment of canisters Nos. 1 through 8 to begin 2800 feet short of the scheduled position. Deployment began at H-137 seconds and concluded at H-51 seconds. The positions of the canisters at shock arrival time are compared with the intended positions in Figure 2.2. Much of the error in placement can be explained by error in drop position. What appears to be a great error is actually the result of lengthening the entire array pattern to compensate for the high wind condition at shot time.

2.3.3 Canister Operation

Pressure data were not recorded for canister No. 7 because of failure of the canister's internal power supply. Data from the No. 9 position were not recorded because the drift measurement canister dropped in this position had no telemetry equipment installed. The 28-foot parachute on canister No. 14 failed to open, resulting in a free fall and impact time of H-19 seconds; all other parachutes deployed satisfactorily. Signals from canister No. 11 (positioned at 8000 feet MSL and 4500 feet slant range from ground zero at zero time) terminated at H+10 seconds. The canister could not be found after the test and may have been damaged both by thermal radiation and the shock wave. All other canisters survived the shock wave and thermal radiation, however, the blue and black stenciled markings were burned on the 28-foot white parachutes of canisters Nos. 4, 12, and 13.

Four canisters, identical in instrumentation to the parachute-borne canisters, were placed on the ground at various ranges from ground zero. Pressure data were recorded from canisters 2G and 4G but no data were obtained from canisters 1G and 3G because of battery power failure.

2.3.4 Radio Telemetry Operation

The ground radio telemetry station recorded pressure data from canisters Nos. 1, 2, 3, 4, 5, 6, 8, 10, 12, 13, 15, 16, 2G and 4G. The canister RF carriers were recorded from time of deployment to H+10 minutes except for the 2 second period when the base power failed after

TABLE 3.8

detonation time. This failure caused the loss of some data of blast wave arrival time from canister No. 11, and only the negative phase of the blast wave was recorded.

2.3.5 Multiple Object Tracking System (MOTS) Operation

The MOTS stations M1A, M2A, and R1 initiated recording procedures at H-1 minute. The manned stations M1A and M2A recorded canister positional data until H+6 minutes. The remotely controlled station, R1, recorded from H-1 minute until shock wave arrival time at H+6 seconds, at which time remote control holding relays failed.

2.4 OPERATION SHOT 8

The problems of the operation were identical to Shot 5. The location of the radio telemetry station, the MOTS stations, and the SCR 584 radar station are indicated in Figure 2.3.

2.4.1 Low Aircraft Operation

The low aircraft operated at 24,400 ft. MSL at a true ground speed of 340 feet per second. Seven practice runs were made between H-4 hours and H-30 minutes, and a canister was deployed at H-2½ hours and H-1½ hours for the purpose of checking drift calculations. The information received checked the calculated drift figure. In the operation run the aircraft was 1 second early resulting in a positional error of 350 feet. The scheduled deployment of canisters Nos. 9 through 16 was started at H-175 seconds and concluded at H-47 seconds. The positions of the canisters at shock arrival time are shown in Figure 2.4.

2.4.2 High Aircraft Operation

The high aircraft maintained a speed of 400 feet per second (true ground speed) at an altitude of 31,800 ft. MSL. Between H-4 hours and H-30 minutes, five practice runs were made. The final run was completed with a positional error of 400 feet caused by the aircraft being early at the intended drop point. At H-171 seconds the deployment of canisters Nos. 1 through 8 was begun and it was completed at H-89 seconds. The canister positions at shock arrival time are pictured in Figure 2.4.

2.4.3 Canister Operation

Pressure data were not recorded for canister No. 3 due to

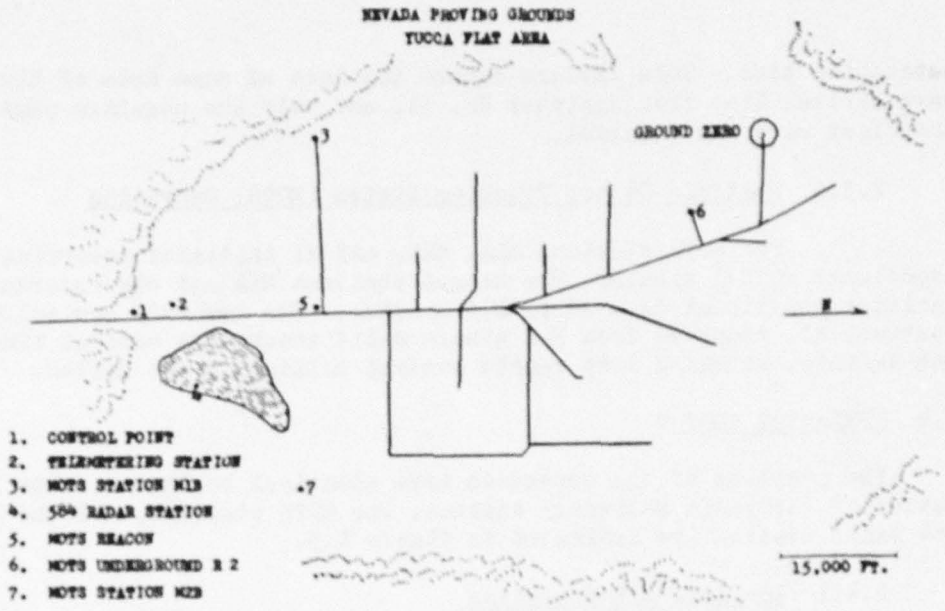

Fig. 2.3 Station Locations for Shot 8

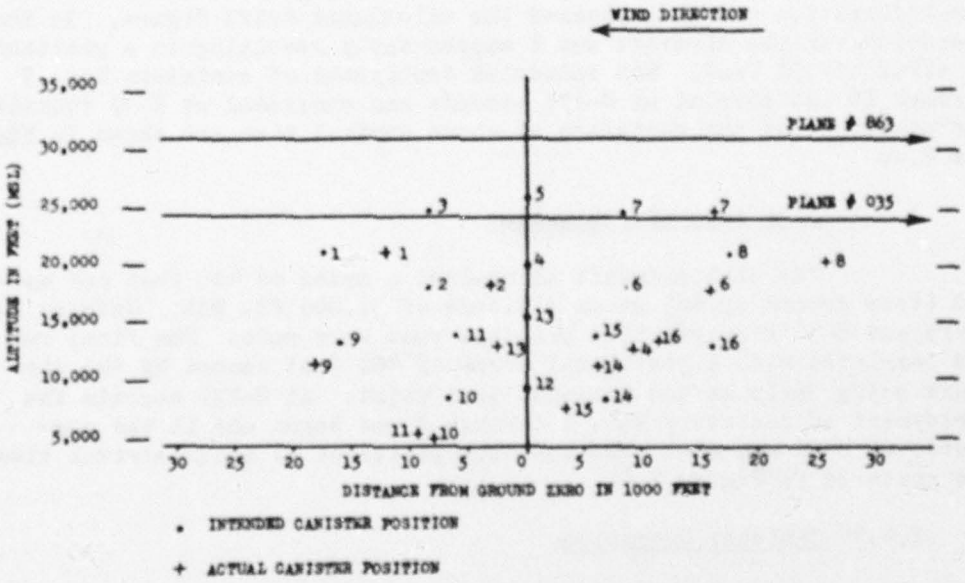

Fig. 2.4 Canister Array for Shot 8

pressure gage malfunction. The large parachute on canister 5 probably did not open since both pressure gages were off scale. Power supply failure in canister 12 prevented proper function of the parachute system, resulting in a free fall and impact time of H-16 seconds.

Four canisters, identical in instrumentation to the parachute-borne canisters, were placed on the ground at various ranges from ground zero. Pressure data were recorded from all ground canisters.

2.4.4 Radio Telemetry Operation

The ground radio telemetry station recorded pressure data from canisters Nos. 1, 2, 4, 6, 7, 8, 9, 10, 11, 13, 14, 15, 16, 1G, 2G, 3G and 4G. The canister RF carriers were recorded from time of deployment to H+10 minutes. Power was obtained from PE-95 units in order to avoid base power failure at zero time.

2.4.5 Multiple Object Tracking System (MOTS) Operation

MOTS stations M1B, M2B and R2 initiated recording procedures at H-1 minute. All stations recorded canister positional data to H+6 minutes.

2.4.6 Canister Test Damage Operation

In an attempt to determine the effects of thermal radiation and shock blast on the canisters, three canisters were located at distances of 300, 800 and 1500 feet from ground zero. The canisters were placed in a vertical position at each location and were braced with four 1/8 inch steel cables. Investigation of the canisters at H+3 days indicated that the nearest canister was completely demolished and parts scattered to distances of 1000 feet from ground zero. All pieces showed evidence of being exposed to extremely high temperatures. The nose and center section of the canister located 800 feet from ground zero were found at separate locations 2000 feet from ground zero. These sections did not show evidence of extreme damage from thermal radiation. The after section of this canister was not located. The canister located at 1500 feet from ground zero was found lying on the ground 10 feet from the guyed position. The antenna was broken and the paint on the outside frame facing ground zero was scorched. No damage was discovered to any internal instrumentation after a laboratory test was completed. The nylon straps attached to the outside of the after section were partially melted.

[redacted]

CHAPTER 3

TEST RESULTS

3.1 SHOT 5

3.1.1 Canister Positions

Although some reliable MOTS data were obtained on Shot 5, they were, in general, insufficient to determine accurate canister positions at shock arrival time without additional data from other sources. It was accordingly decided to use the canister altimeters and the measured time of fall for the determination of altitude and use the measured shock travel time for the determination of slant range, with the MOTS data used as a check. Table 3.1 shows the canister altitudes at shock arrival time as determined by (a) telemetered ambient pressure converted to true altitude in accordance with the radiosonde meteorological data for the time of the shot and by (b) the times of fall on both small and large parachutes taken in conjunction with the previously calibrated rates of descent and the known altitudes of the drop aircraft. The means of these two, when both were determined, are taken as the best estimates of canister altitudes. The arithmetic mean of the percentage difference between the two, which may be taken as a rough measure of the accuracy of the altitude data, is 4.4 per cent.

The slant ranges computed from the shock travel times by the method described in Appendix A are given in the second column of Table 3.2. From the more complete MOTS data obtained on Shot 8 the algebraic mean difference between the travel time ranges and the MOTS ranges was found to be +2.18 per cent. Since the MOTS ranges for Shot 8 are considered to be less subject to possible small systematic errors than the travel time ranges, this is interpreted as indicating a systematic error of +2.18 per cent in the method used for computing slant range from travel time. The third column of Table 3.2 gives the travel time ranges reduced by 2.18 per cent and the fourth column gives the ranges as computed from the MOTS data used in conjunction with the drop-time altitudes* given in column 3 of Table 3.1. However, in view of the uncertainty in much of the MOTS data for this shot, the reduced travel time ranges (column 3) are taken as the best values except in the case of canister No. 13, for which this range is inconsistent with the altitude. In this case the MOTS data has been used.

*The MOTS computations were carried out before the correct altimeter altitudes were available. Since use of the final altitude figures would not alter the MOTS ranges significantly, these ranges have not been recomputed.

[redacted]

TABLE 3.1

Canister Altitudes at Shock Arrival Time, SHOT 5

Canister (1)	Altitude (ft. above M.S.L.)		
	From Canister Altimeter (2)	Computed from Drop Time (3)	Mean (4)
1	22,680	25,000	23,840
2	23,000	22,750	22,880
3	27,150	29,780	28,470
4	17,520	17,440	17,480
5	31,420	30,340	30,880
6	22,100	21,460	21,780
8	26,680	26,620	26,650
10	14,780	no data	14,780
11	no data	6,960	6,960
12	7,300	8,740	8,020
13	13,500	13,500	13,500
15	14,410	14,520	14,470
16	15,100	15,460	15,280

In addition to the parachute-borne gages, shock pressure measurements were obtained from two of the four ground canisters. The slant ranges from the bomb were 6810 feet for Station 2G and 17,470 feet for Station 4G.

3.1.2 Shock Wave Data

The telemetered records of shock overpressures as functions of time are shown in Figure 3.1. These records are reproduced from the traces on the original telemetering records of Shot 5, Figure 3.2. The principal numerical data are summarized in Table 3.3. Small secondary

TABLE 3.2

Slant Ranges at Shock Arrival Time, SHOT 5

Canister (1)	Slant Range from Bomb (ft.) Computed from: Travel Time (2)	Column (2) less 2.18% (3)	MOTS with Assumed Altitude (4)
1	33,250	32,530	32,900
2	25,420	24,870	25,150
3	31,640	30,950	32,000
4	15,190	14,860	14,950
5	28,390	27,770	27,750
6	20,080	19,640	18,500
8	28,600	27,980	25,250
10	13,040	12,760	-
12	5,240	5,125	5,500
13	8,700	8,510	9,100
15	14,810	14,490	13,350
16	22,980	22,480	19,050

shocks appear on the traces from canisters Nos. 2, 5, and 13. That from canister No. 2 appears in the negative pressure phase of the main shock, but it is questionable whether this represents incipient development of the tail shock since it is not found on traces from still larger distances. The secondary shocks observed on canisters Nos. 5 and 13, arriving 0.26 and 0.67 seconds respectively after the main shock, are not considered to represent the main ground reflection since they do not appear on the traces from intermediate and shorter distances. In particular, the nearest canister, No. 12, shows no indication of a double peak. It is therefore assumed that the direct and main reflected shocks have coalesced into a single Mach shock at all canister positions.

3.2 SHOT 8

3.2.1 Canister Positions

The canister altitudes at shock arrival time as given by the MOTS data, canister altimeters (corrected for prevailing meteorological conditions), and computation from drop time and rates of descent are given in Table 3.4. The last column in the table gives the preferred values used in further discussion of the data.

For canisters Nos. 1 and 2 no record was obtained of the time of release from the aircraft, and for canisters Nos. 4, 10, and 11 the altitudes computed from the drop times were so much greater than the MOTS and altimeter altitudes that it was evident that the parachutes failed to open properly and standard rates of descent could not be applied.

The slant ranges at shock arrival time determined from the MOTS data (R_{MOTS}) and by computation from the observed travel times (R_{TT}) are given in Table 3.5 together with the percentage difference between the two. Since there is no apparent reason to expect a systematic error in the MOTS ranges, the fact that the travel time ranges tend to be larger is taken as indicating a small systematic error in the method used in computing the travel time ranges. The algebraic mean percentage difference, including the ground Stations 2G, 3G, and 4G, is +2.18 per cent, and this figure has been applied as a correction to the travel time ranges for Shot 5. Ground Station 1G, which shows a relatively large difference of opposite sign, has been omitted in computing the mean, since at short distances the computation of range from travel time is relatively more sensitive to the assumed form of the overpressure vs. distance curve in the high overpressure region, and there is also the possibility that the shock velocity may be abnormally high near the ground at short ranges because of the pre-heating of the air by thermal radiation.

3.2.2 Shock Wave Data

The telemetered shock overpressures as a function of time after the explosion are shown in Figure 3.3. Figure 3.4 is a sample trace from the telemetered records of Shot 8. The principal numerical data are summarized in Table 3.6. The occurrence of small secondary shocks is more frequent than in the case of Shot 5, but again there is no correlation from one position to another, suggesting that they may be caused by inter-action of the main shock and turbulent motions of relatively small extent in the atmosphere.

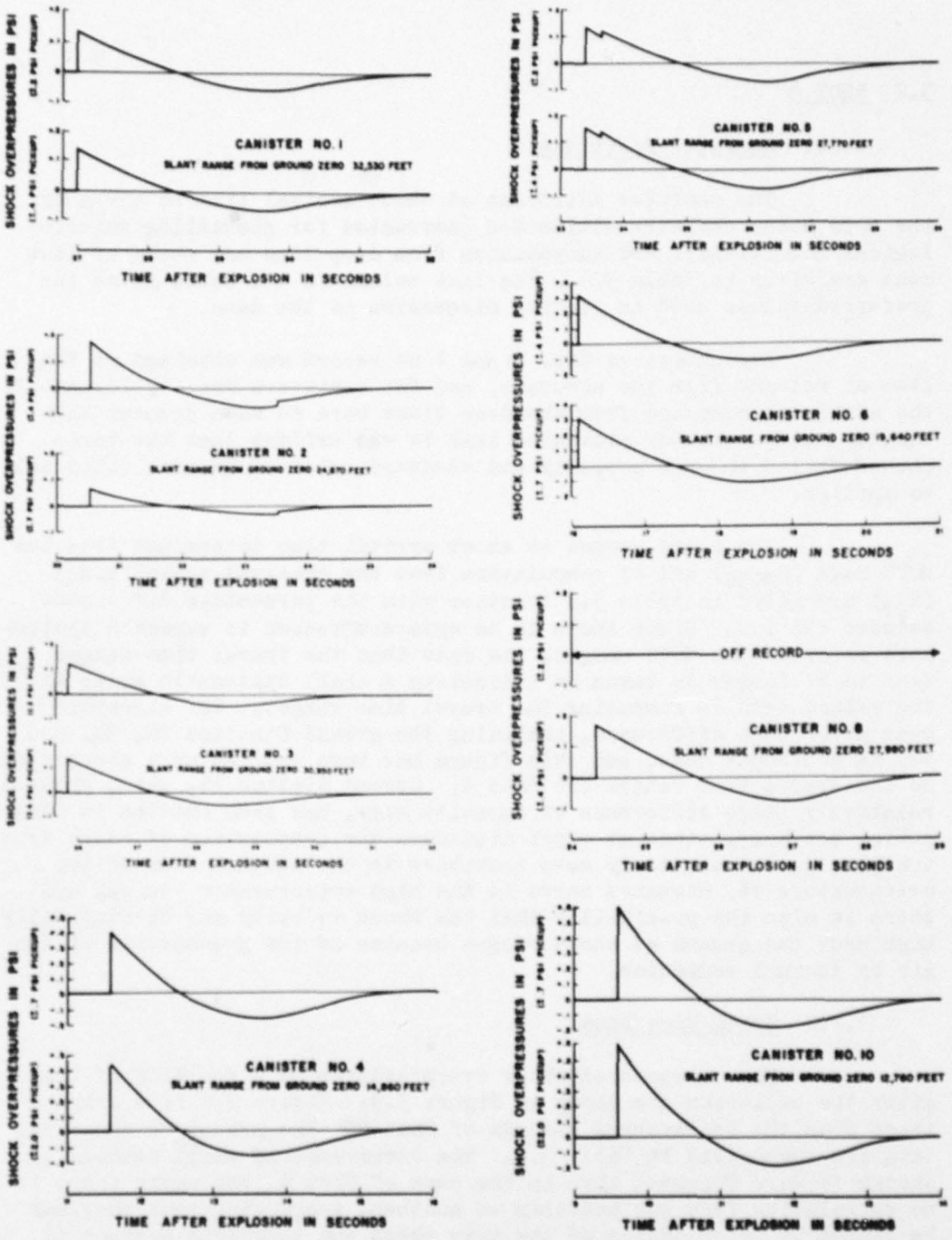

Fig. 3.1 - Shock Overpressure vs. Time - Shot 5

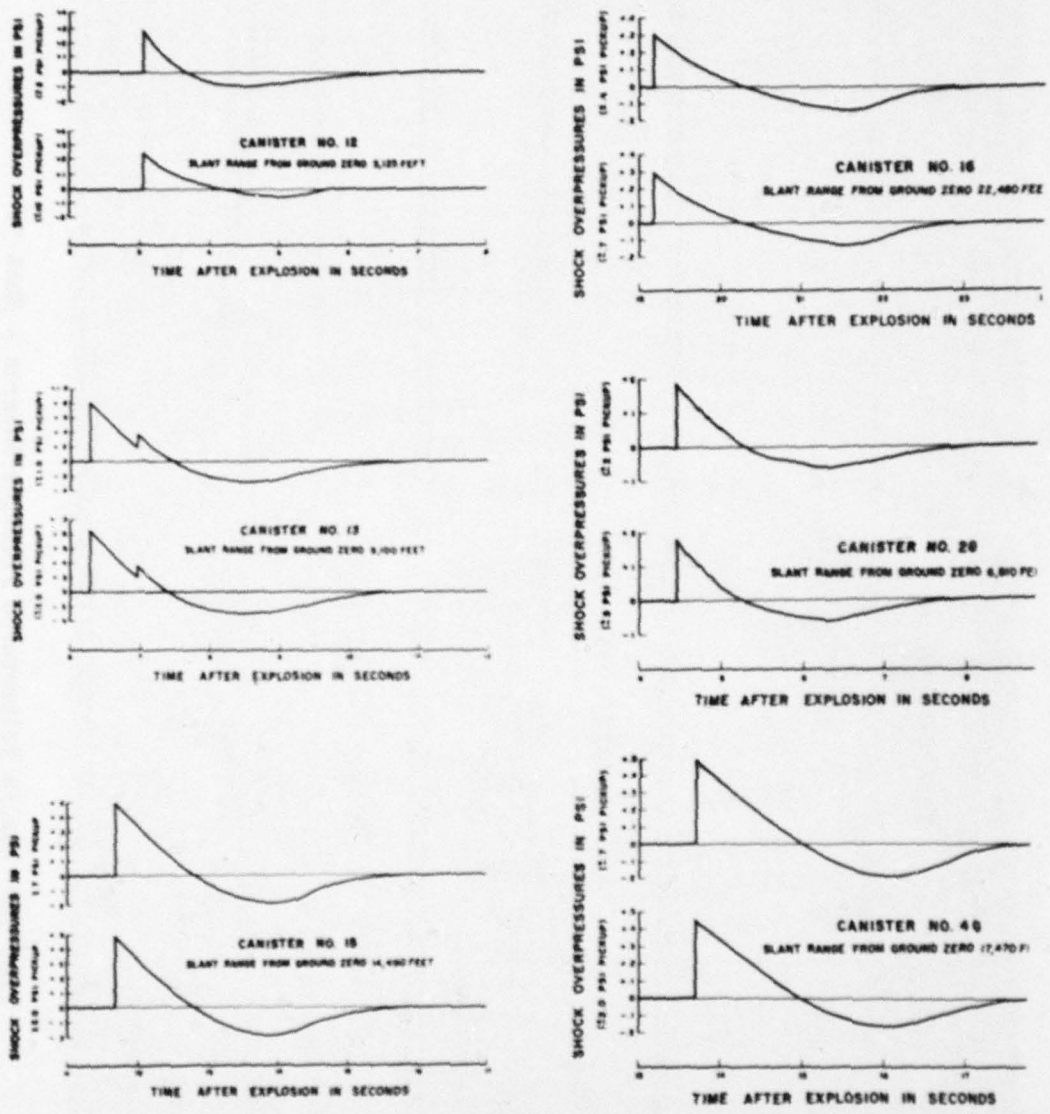

Fig. 3.1 continued - Shock Overpressure Vs. Time - Shot 5

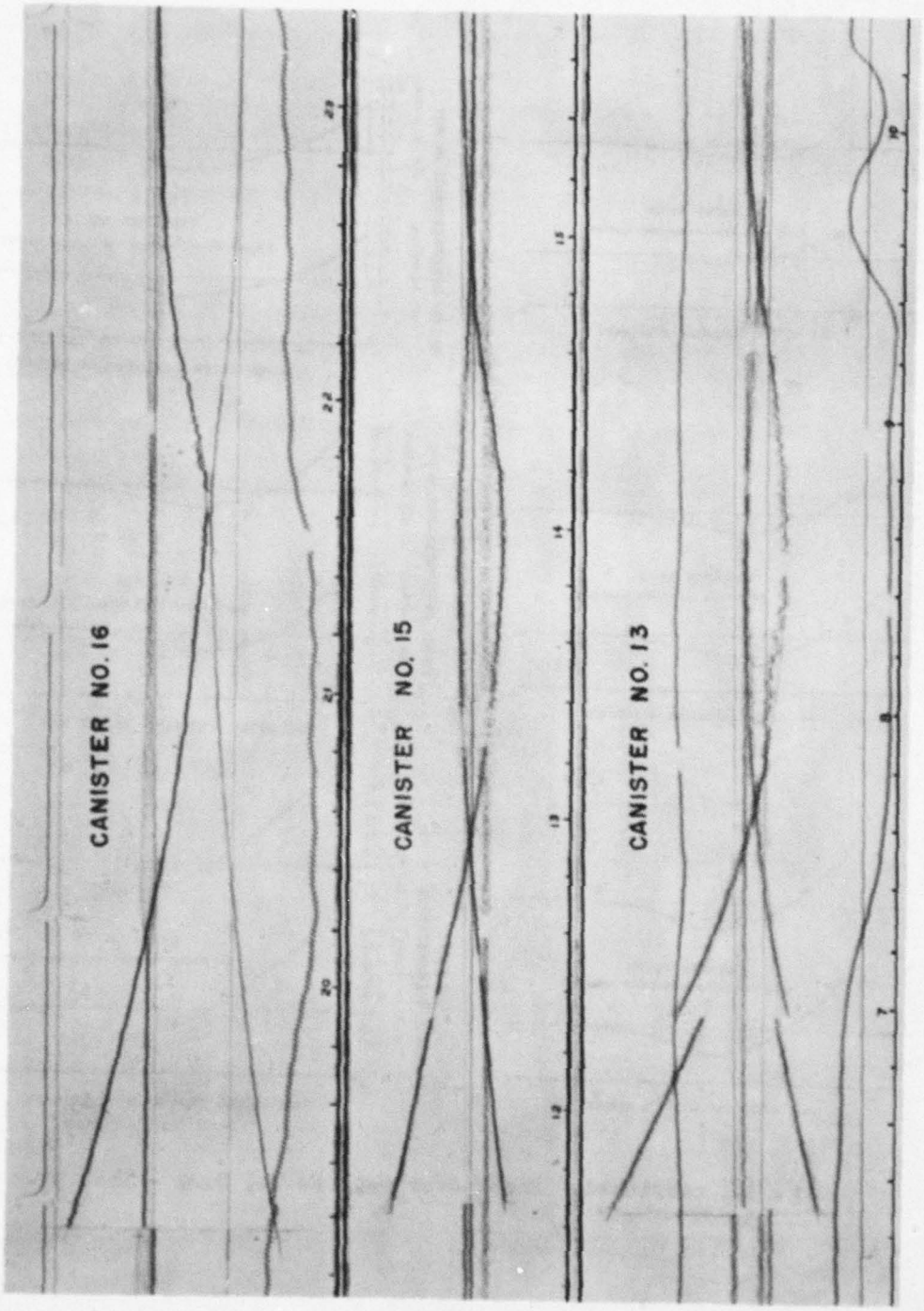

Fig. 3.2 Sample Telemetered Pressure Records - Shot 5

TABLE 3.3

Shock Wave Data - Shot 5

Canister No.	Peak Overpressure (psi)			Max. Underpressure (psi)			Shock Arrival time (sec)	Duration of Positive Overpressure (sec)
	High Range Gage	Low Range Gage	Mean	High Range Gage	Low Range Gage	Mean		
1	0.145	0.137	0.141	-0.061	-0.056	-0.059	26.99	1.45
2	gross error	0.175	0.175	gross error	-0.075	-0.075	20.52	1.22
3	0.135	0.120	0.128	-0.048	-0.050	-0.049	25.81	1.45
4	0.45	0.40	0.425	-0.155	-0.170	-0.163	11.58	0.94
5	0.157	0.136	0.147	-0.073	-0.071	-0.072	23.37	1.49
6	0.308	0.312	0.310	-0.1021	-0.120	-0.112	16.09	1.27
8	0.168	--	0.168	-0.082	--	-0.082	24.34	1.32
10	0.599	0.609	0.604	-0.182	-0.182	-0.182	9.59	1.17
12	2.48	2.90	2.69	-0.52	-0.93	-0.73	3.05	0.87
13	0.827	0.807	0.817	-0.294	-0.276	-0.285	6.28	1.13
15	0.483	0.490	0.486	-0.190	-0.187	-0.189	11.68	1.12
16	0.300	0.313	0.307	-0.133	-0.140	-0.137	19.17	1.12
20	1.80	1.90	1.85	-0.60	-0.60	-0.60	4.46	0.83
40	0.45	0.48	0.465	-0.18	-0.19	-0.185	13.69	1.29

TABLE 3.4

Canister Altitudes at Shock Arrival Time, Shot 8

Canister No.	MOTS	Altitude (ft. above M.S.L.)		
		Altimeter	Drop Time	Preferred Values
1	21,950	21,960	-	21,950
2	18,900	19,190	-	18,900
3	25,750	-	24,650	25,750
4	13,400	14,120	-	13,760
6	17,750	18,550	18,200	18,150
7	25,350	25,920	24,700	25,630
8	21,300	20,880	21,500	21,300
9	12,300	13,620	13,450	12,960
10	5,000 (?)	5,480	-	5,240
11	5,700 (?)	6,720	-	6,210
13	-	13,700	13,400	13,700
14	-	14,750	11,050	12,900
15	7,200	7,180	8,500	7,200
16	13,600	14,410	14,000	14,000

3.3 DISCUSSION

3.3.1 Shot 5

The primary objective of the present measurements was to test the validity of the Fuchs[2] scaling law for computing the effect on shock overpressures of the variation of atmospheric pressure and temperature with altitude. To accomplish this we use the Fuchs and

---

[2] K. Fuchs - Los Alamos Technical Series LA-1021, Vol VII, Pt. II, Chapter 9.

TABLE 3.5

Slant Ranges at Shock Arrival Time, Shot 8

Canister No.	MOTS range (R_{MOTS})	Travel Time Range (R_{TT})	$\frac{R_{TT} - R_{MOTS}}{R_{TT}} \times 100$	Preferred Value
1	20,700	21,480	+3.6	R_{MOTS}
2	14,150	14,610	+3.1	14400 (Alt-4500)
3	20,900	21,950(?)	+4.8	R_{MOTS}
4	12,950	13,420	+3.5	"
6	19,950	20,340	+1.9	"
7	25,750	26,600	+3.2	"
8	30,800	31,560	+2.4	"
9	19,500	19,910	+2.1	"
10	8,050(?)	8,270	+2.7	"
11	9,200	9,410	+2.2	"
13	-	9,290		9200 (Alt-4500)
14	-	9,530		9320 (R_{TT} less 2.18%)
15	4,550	4,940	+7.9	R_{MOTS}
16	14,900	14,930	+0.2	"
Ground Station	Surveyed Range			
1G	3,710	3,160		R(Surveyed)
2G	5,410	5,240	+3.2	"
3G	10,200	9,950	+2.5	"
4G	17,500	17,640	+0.8	"
Algebraic mean percentage diff. +2.18				

Sachs[3] scale factors to scale the observed values of pressure and range to equivalent values in an idealized isothermal atmosphere at constant ambient pressure of 14.70 psi. If the theory is valid, the scaled overpressure should be a function only of the scaled range. We introduce the following notation:

ΔP = Peak overpressure. (psi.)

R = Slant range. (ft.)

z = Altitude at which ΔP is measured. (ft. above MSL)

h = Altitude of bomb. (ft. above MSL)

W = Yield of bomb (KT), including reflection factor

P_o = Ambient atmospheric pressure (psi.)

T = Ambient atmospheric temperature (° Absolute)

$S = W^{1/3}$ = Yield scale factor (relative to 1 KT)

$k = \left[P_o(h)/P_o(o)\right]^{1/3}$ = Sachs scale factor

$\lambda = \exp\int_z^h \left[\left\{T(h)/T(z)\right\}^{3/4}\left\{P_o(h)/P_o(z)\right\}^{1/2}-1\right] dz/(z-h)$ } Fuchs Scale Factors

$\mu = \lambda\left\{T(h)/T(z)\right\}^{1/4}\left\{P_o(z)/P_o(h)\right\}^{1/2}$ } Fuchs Scale Factors

$\Delta P/k^3\mu$ = Scaled overpressure

$r = k\lambda R/S$ = Scaled range (relative to 1 KT)

The scale factors λ and μ, which are tabulated as functions of altitude in Appendix C, have been computed by numerical integration using the radiosonde meteorological data taken at the time of the shot as given in Appendix B. The best estimate of the radiochemical yield of Shot 5 presently available to the writer is 11.7 KT. A reflection factor of 1.8 will be assumed. This is an arbitrary choice, but one which appears to make the present data reasonably consistent with measurements taken by other methods at higher overpressures. We then have $S = (11.7 \times 1.8)^{1/3} = 2.761$. The scaled overpressures and

---

3/ R. G. Sachs - The Dependence of Blast on Ambient Temperature and Pressure, Ballistic Research Laboratories, Aberdeen Proving Ground, Report #466 (May 1944)

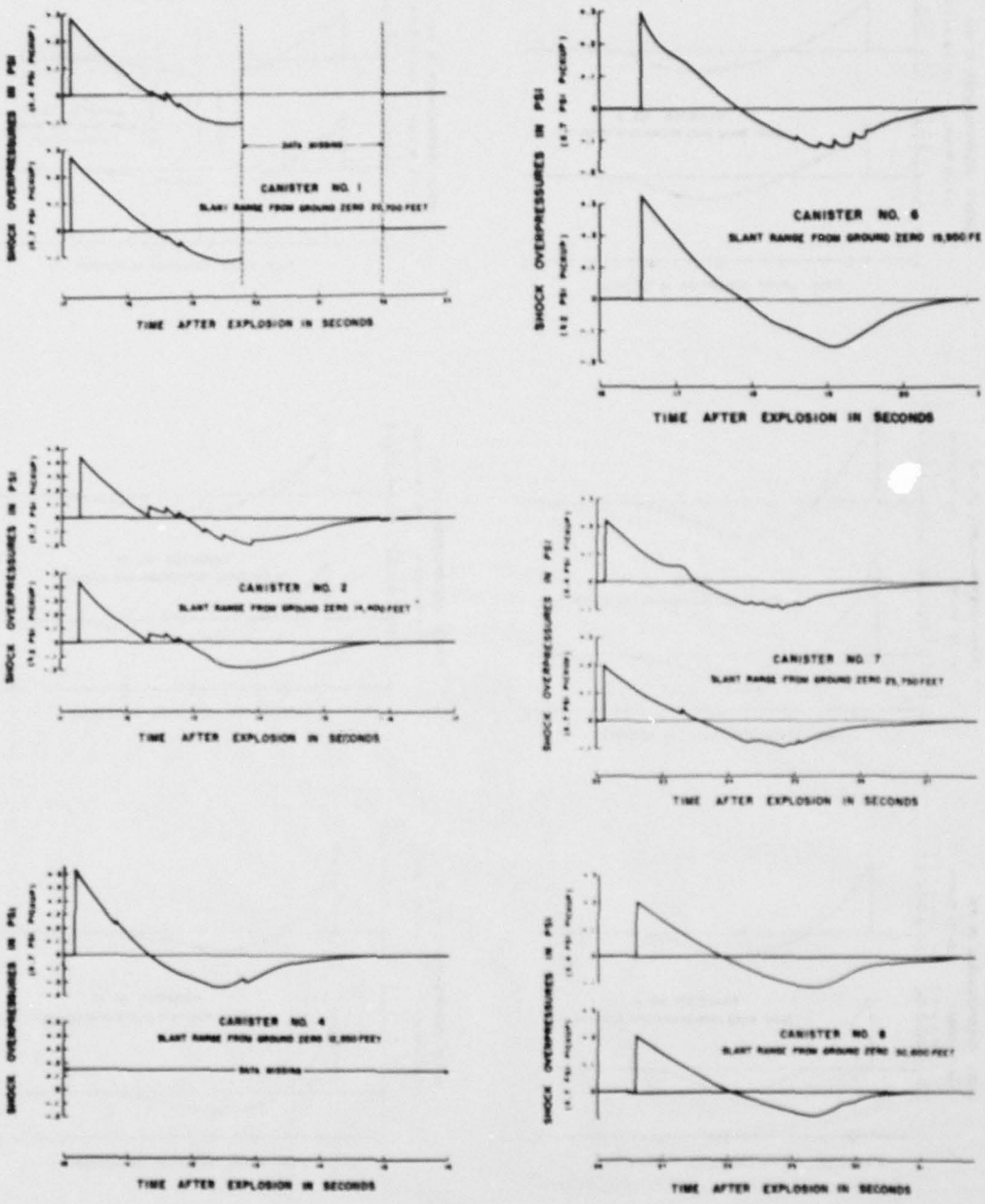

Fig. 3.3 - Shock Overpressure vs. Time - Shot 8

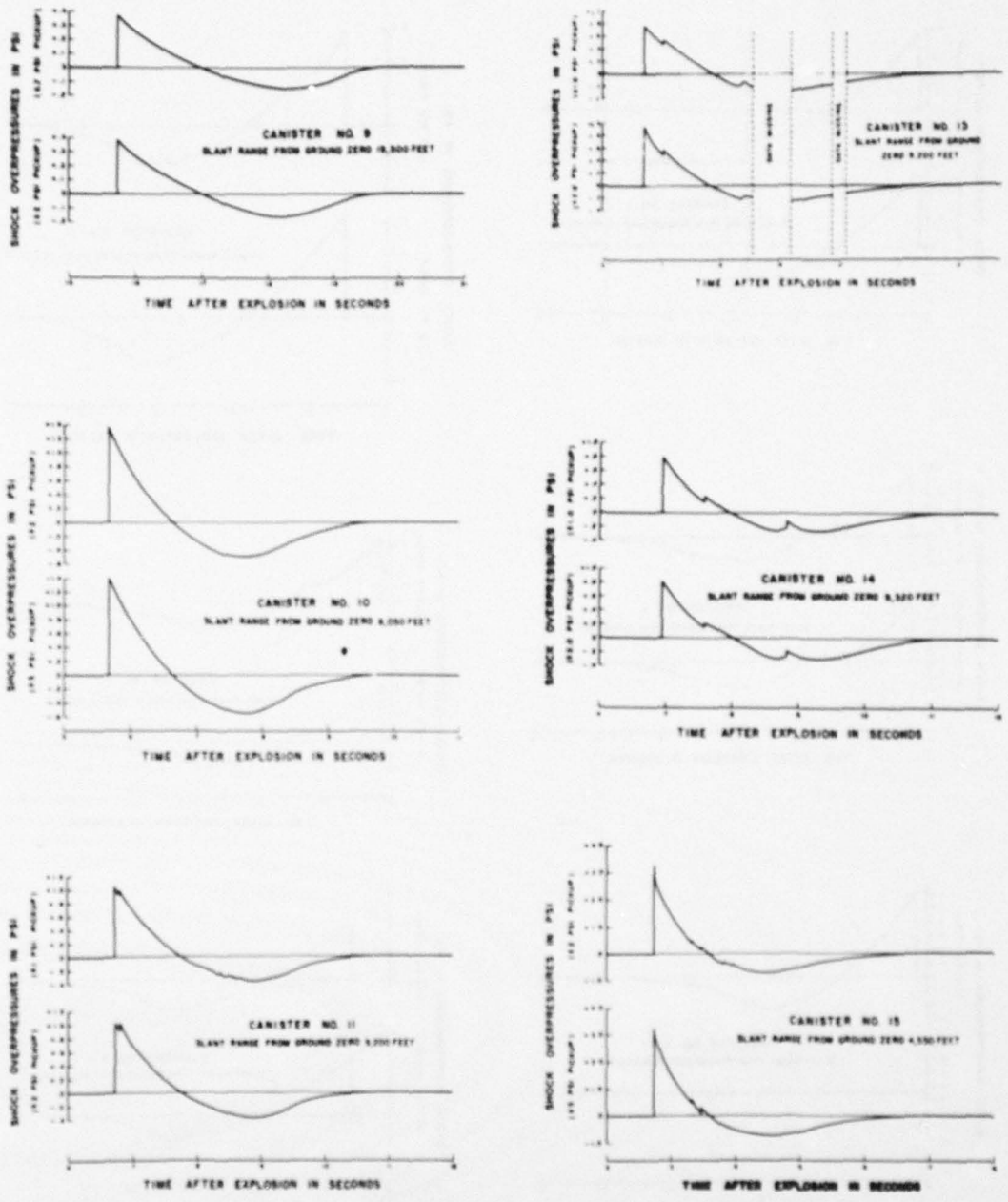

Fig. 3.3 continued - Shock Overpressure vs. Time - Shot 8

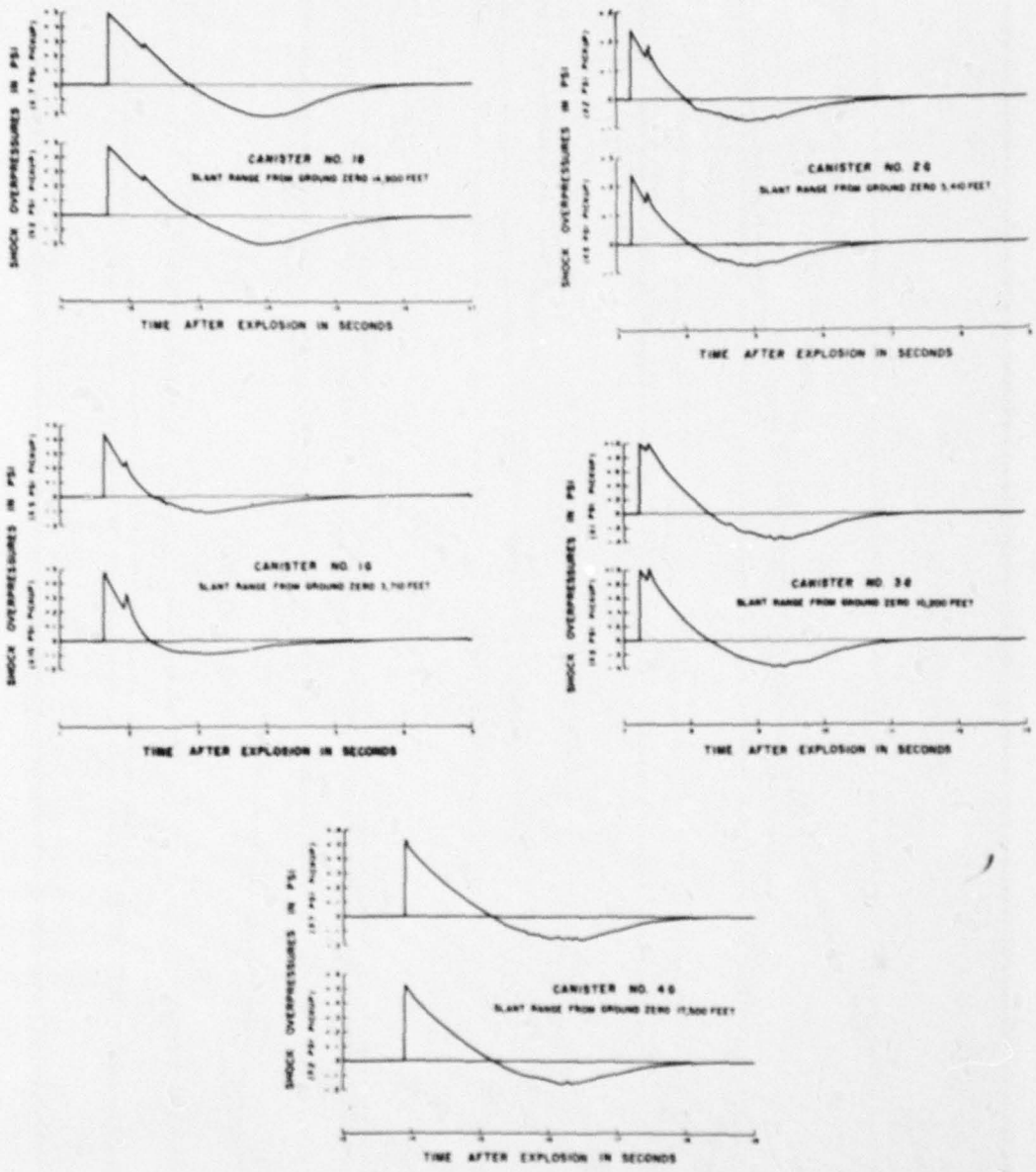

Fig. 3.3 continued - Shock Overpressure vs. Time - Shot 8

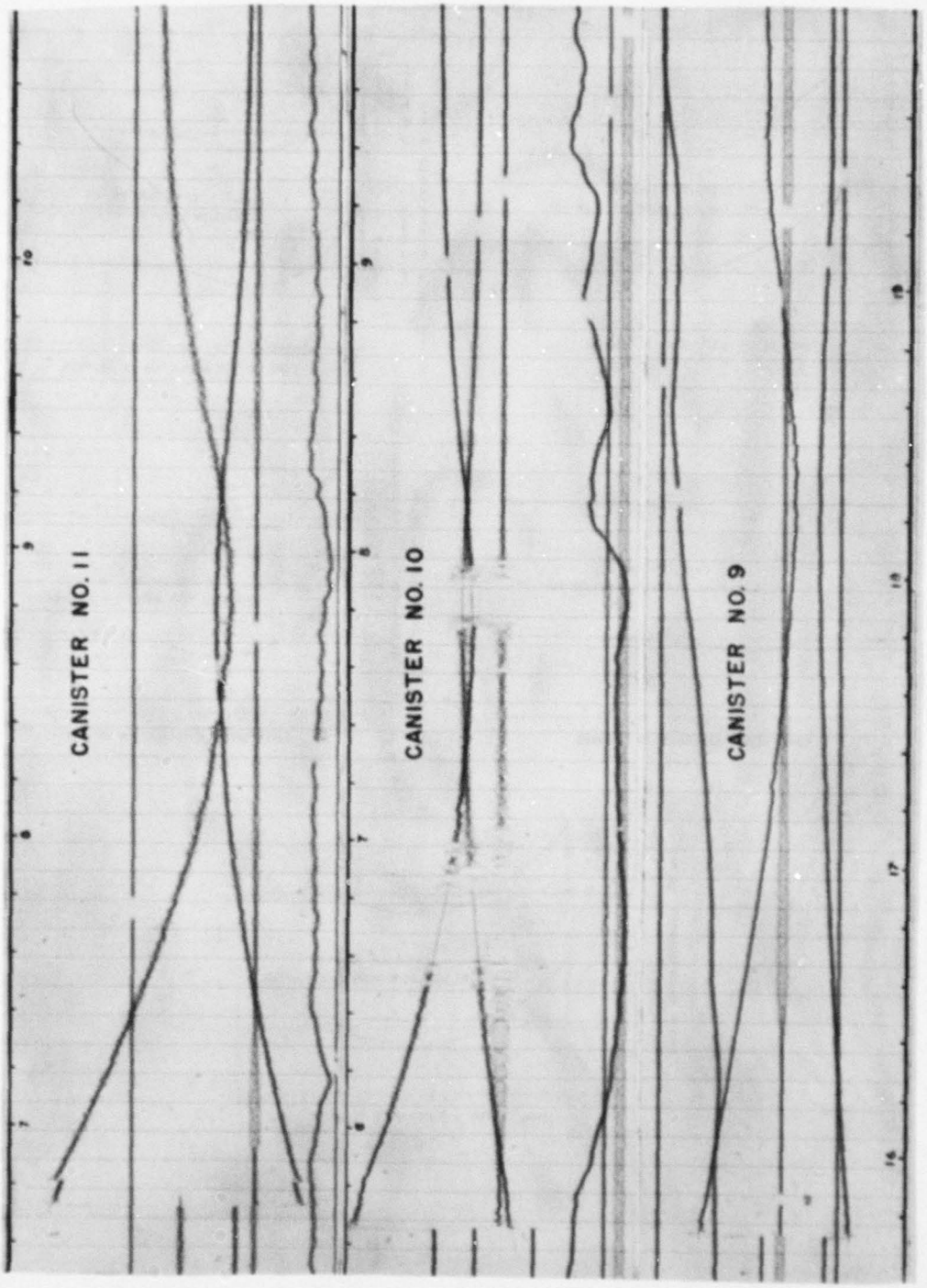

Fig. 3.4 Sample Telemetered Pressure Records - Shot 8

TABLE 3.6

Shock Wave Data – Shot 8

Canister No.	Peak Overpressure (psi)			Max. Underpressure (psi)			Shock Arrival Time (sec)	Duration of Positive Overpressure (sec)
	High Range Gage	Low Range Gage	Mean	High Range Gage	Low Range Gage	Mean		
1	0.267	0.284	0.276	-0.116	-0.108	-0.112	17.13	1.32
2	0.43	0.44	0.435	-0.18	-0.194	-0.187	11.27	1.07
3	-	-	-	-	-	-	17.56	-
4	-	0.624	0.624	-	-0.204	-0.204	10.17	1.17
6	0.327	0.300	0.314	-0.150	-0.116	-0.133	16.55	1.33
7	0.199	0.214	0.207	-0.096	-0.099	-0.098	22.13	1.40
8	0.206	0.205	0.205	-0.091	-0.114	-0.103	26.59	1.41
9	0.375	0.365	0.370	-0.160	-0.149	-0.154	15.73	1.27
10	1.40	1.36	1.38	-0.55	-0.48	-0.515	5.67	0.97
11	1.020	1.045	1.033	-0.370	-0.362	-0.366	6.73	1.03
13	0.850	0.770	0.810	-	-	-	6.71	1.15
14	0.810	0.790	0.800	-0.290	-0.270	-0.280	6.95	1.05
15	3.22	3.25	3.235	-0.736	-0.719	-0.727	2.74	0.85
16	0.480	0.495	0.488	-0.194	-0.213	-0.204	11.68	1.21
1G	4.80	4.42	4.61	-1.0	-1.10	-1.05	1.64	0.68
2G	2.42	2.38	2.40	-0.77	-0.75	-0.76	3.22	0.84
3G	1.00	1.00	1.00	-0.37	-0.36	-0.365	7.24	1.06
4G	0.525	0.525	0.525	-0.160	-0.160	-0.160	13.89	1.28

ranges are given in Table 3.7 and plotted in Figure 3.5. The solid comparison curve plotted in the figure is defined by the expressions:

$$f(r) = \frac{1561 \times 10^6}{r^3} + \frac{246.9 \times 10^4}{r^2} + \frac{3026}{r} \quad \text{for } f(r) > 1 \text{ psi} \qquad (3.1)$$

$$f(r) = 3650/r\sqrt{\log_{10}(r/446.7)} \quad \text{for } f(r) < 1 \text{ psi.} \qquad (3.2)$$

r = Scaled range in feet.

This curve is not intended to represent an attempt at a "best fit" to the present data, but was derived as described in a previous report on the preliminary parachute gage measurements carried out at the JANGLE surface shot[4/]. Omitting the ground stations, the root mean square percentage deviation of the observed overpressure from the comparison curve is 11.5 per cent and the algebraic mean percentage difference is -2.7 per cent. The r.m.s. deviation from some hypothetical "true" or "best fitting" curve would not be larger than that obtained by removing the systematic component, or $\sqrt{(11.5)^2 - (2.7)^2} = 11.2$ per cent.

3.3.2 Shot 8

The scale factors λ and μ computed for the meteorological conditions prevailing at the time of Shot 8 are tabulated in Appendix C. The yield for this shot is taken to be 14 KT, which, with a reflection factor of 1.8, gives $S = (14 \times 1.8)^{1/3} = 2.932$. The scaled data for this shot are tabulated in Table 3.8 and plotted in Figure 3.6 with the same comparison curve defined by equations (3.1) and (3.2). Omitting the ground stations, the r.m.s. percentage deviation from the comparison curve is 8.4 per cent and the algebraic mean percentage deviation is - 3.8 per cent. Removing the systematic component, the resultant is 7.5 per cent.

4/ N. A. Haskell, J. O. Vann, The Measurement of Free Air Atomic Blast Pressures, Operation JANGLE, Project 1.3c, Air Force Cambridge Research Center

TABLE 3.7

Overpressures and Ranges Scaled to 1 KT in a Homogeneous Unbounded Atmosphere at 14.70 psi Ambient Pressure, Shot 5

h = 4500 ft., k^3 = 0.854, k = 0.948, S = 2.761							
Canister No.	Range R	Altitude z	Peak Overpressure ΔP	Scale Factors λ	μ	Scaled Range $r = \lambda R/S$	Scaled Overpressure $\Delta P/k^3$
1	32,530	23,840	0.141	1.709	1.277	19,070	0.129
2	24,870	22,880	0.175	1.655	1.203	14,120	0.170
3	30,950	28,470	0.128	2.012	1.317	21,360	0.113
4	14,860	17,480	0.425	1.399	1.124	7,130	0.443
5	27,770	30,880	0.147	2.206	1.371	21,010	0.125
6	19,640	21,780	0.310	1.597	1.185	10,760	0.306
8	27,980	26,650	0.168	1.883	1.277	18,070	0.154
10	12,760	14,780	0.604	1.293	1.088	5,660	0.650
12	5,125	8,020	2.69	1.080	1.016	1,900	3.10
13	9,100	13,500	0.817	1.246	1.073	3,890	0.892
15	14,490	14,470	0.486	1.281	1.084	6,370	0.525
16	22,480	15,280	0.307	1.311	1.094	10,110	0.328
20	6,810	4,200	1.85	1.000	1.000	2,335	2.17
40	17,470	4,200	0.465	1.000	1.000	5,990	0.544

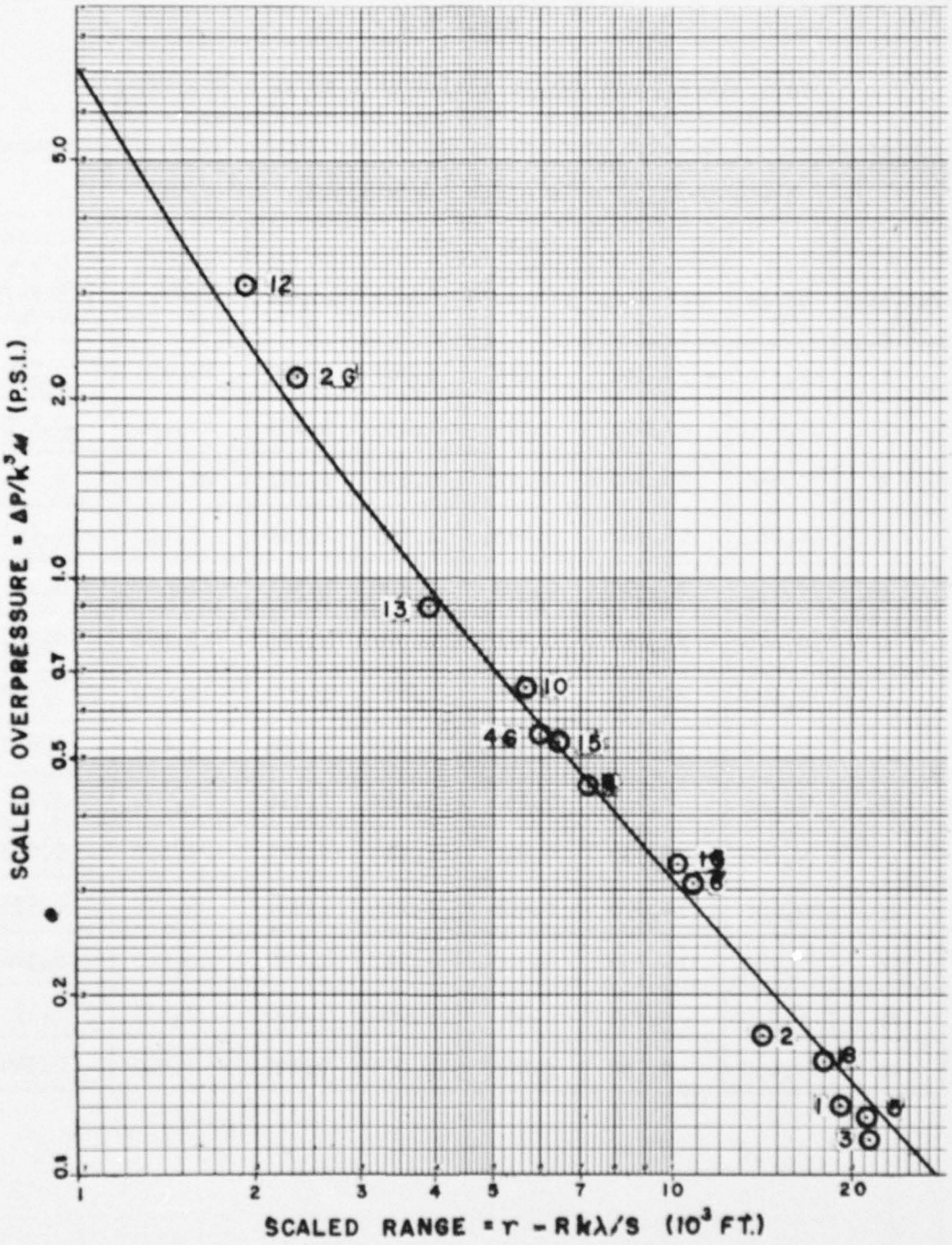

Fig. 3.5 Overpressure vs. Range Reduced to 1 KT in an Unbounded, Homogeneous Atmosphere at 14.70 psi Ambient Pressure - Shot 5

TABLE 3.8

Overpressures and Ranges Scaled to 1 KT in a Homogeneous Unbounded Atmosphere at 14.70 psi Ambient Pressure, Shot 8

h = 4500 ft., k^3 = 0.853, k = 0.948, S = 2.932							
Canister No.	Range R	Altitude z	Peak Overpressure ΔP	Scale Factors λ	Scale Factors μ	Scaled Range $r=k\lambda R/S$	Scaled Overpressure $\Delta P/k^3\mu$
1	20,700	21,950	0.276	1.541	1.138	10,310	0.284
2	14,400	18,900	0.435	1.412	1.104	6,570	0.462
4	12,950	13,760	0.624	1.228	1.053	5,140	0.695
6	19,950	18,150	0.314	1.383	1.096	8,920	0.336
7	25,750	25,630	0.207	1.725	1.192	14,360	0.204
8	30,800	21,300	0.205	1.512	1.130	15,060	0.213
9	19,500	12,960	0.370	1.203	1.046	7,580	0.415
10	8,050	5,240	1.38	1.013	0.999	2,640	1.62
11	9,200	6,210	1.033	1.032	1.002	3,070	1.21
13	9,200	13,700	0.810	1.226	1.052	3,650	0.903
14	9,320	12,900	0.800	1.202	1.046	3,620	0.897
15	4,550	7,200	3.235	1.053	1.007	1,550	3.77
16	14,900	14,000	0.488	1.236	1.055	5,950	0.542
1G	3,710	4,200	4.61	1.000	1.000	1,200	5.40
2G	5,410	4,200	2.40	1.000	1.000	1,750	2.81
3G	10,200	4,200	1.00	1.000	1.000	3,300	1.17
4G	17,500	4,200	0.525	1.000	1.000	5,660	0.615

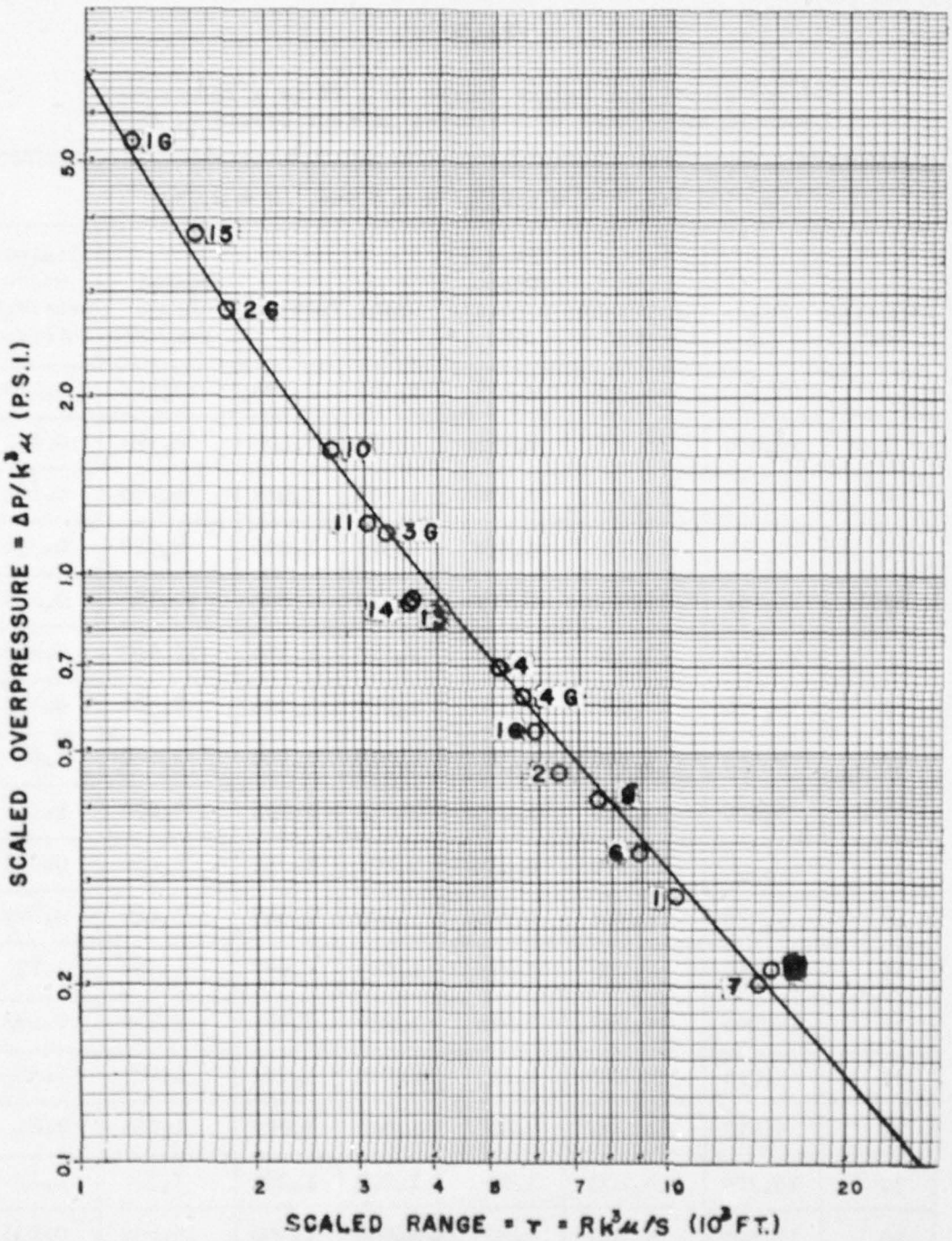

Fig. 3.6 Overpressure vs. Range Reduced to 1 KT in an Unbounded Homogeneous Atmosphere at 14.70 psi Ambient Pressure - Shot 8

CHAPTER 4

CONCLUSIONS AND RECOMMENDATIONS

4.1 CONCLUSIONS

4.1.1 Validity of the Fuchs Altitude Correction

Considering Shots 5 and 8 together, the r.m.s. percentage deviation after removal of the systematic component is 9.5 per cent. This may be regarded as the statistical resultant of errors of measurement and of any effects of atmospheric inhomogeneity that are not correctly taken into account by using the Fuchs scale transformation. While no wholly objective measure of the errors of observations can be given, it seems unlikely that they can have a standard deviation of less than 5 per cent, and they might amount to nearly all the observed scatter. In that case, errors attributable to the use of the Fuchs scale transformation are probably no more than $\sqrt{(9.5)^2 - (5.0)^2} = 8.1$ percent and may be considerably less. In any case we conclude that the theory satisfies practical accuracy requirements for the prediction of peak overpressures within the range of altitudes and overpressures covered by the present data.

4.1.2 Effect of Wind

Since the total amount of air passed over by the shock front in reaching a given distance is slightly greater in the upwind than in the downwind direction, it is to be expected that the peak overpressure at a given distance will be slightly smaller in the upwind direction. In Figure 4.1 the percentage deviation from the comparison curve is plotted against the average component of wind velocity along the direction from explosion to gage, a positive sign being taken for the latter when the average wind component is in the direction of shock propagation and a negative sign when it is in the opposite direction. The deviations show some negative correlation with wind velocity, which is in the opposite sense from that which was to be expected. However, because of the assymetry of the actual canister positions, this apparent correlation could be made to disappear by a slight change in the comparison curve used. It is therefore considered that the real effect of wind in these tests is so small that it is masked by the random scatter of the data.

4.1.3 Free Air Peak Overpressure vs. Distance

Because of the uncertainty in the assumed reflection factor

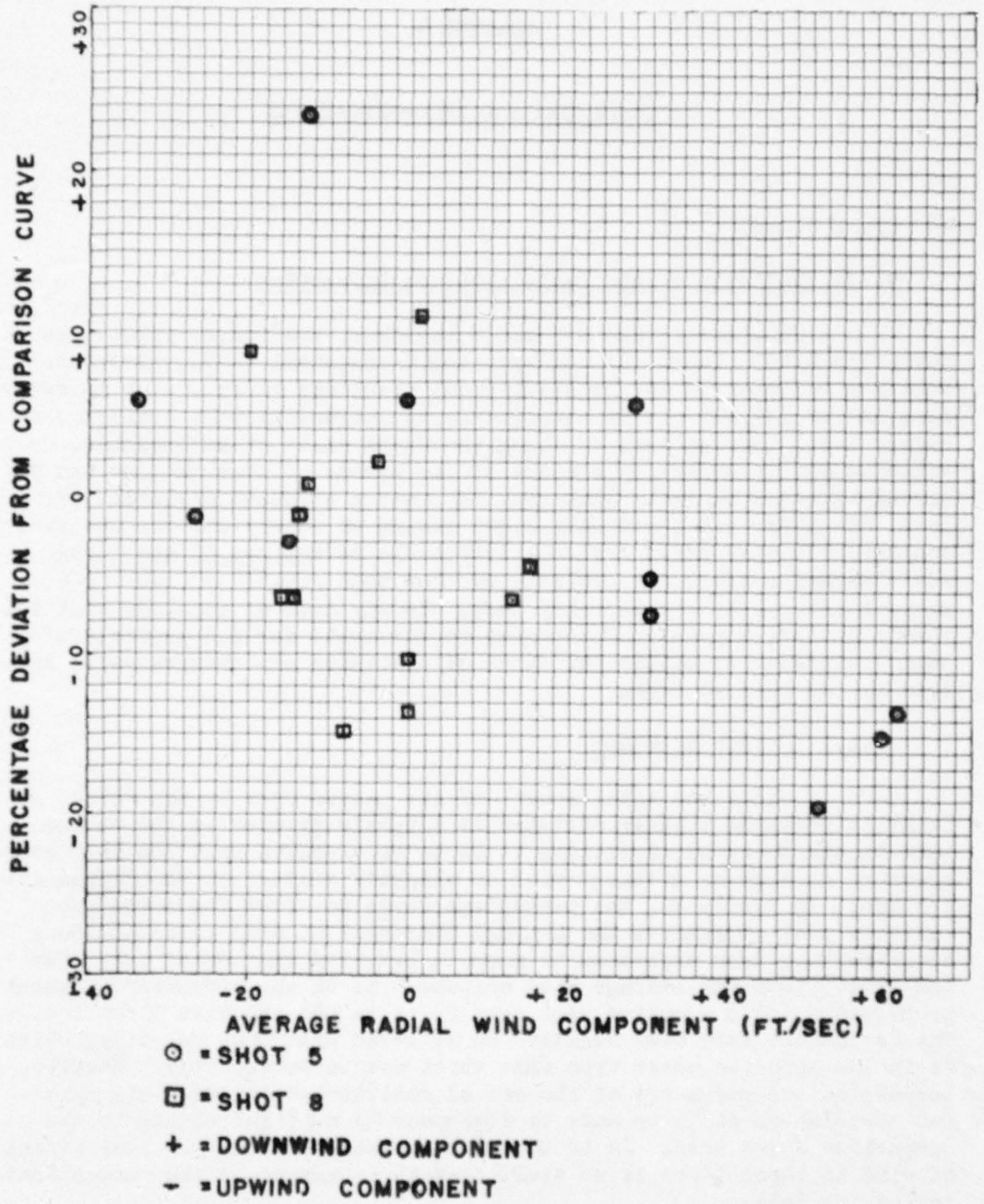

Fig. 4.1 Percentage Deviation from Comparison Curve vs. Average Radial Wind Component

used in reducing the observed data to equivalent free air values for 1 KT, the resultant free air peak overpressure vs. distance curve must be regarded as tentative. Nevertheless, it is of interest to note that the overpressure vs. distance curve given by equation (3.1) is remarkably close to the TUMBLER composite curve based on the Naval Ordnance Laboratory's measurements in the region of high overpressures.[5] The two curves are compared in Figure 4.2. Equation (3.1) falls about 9 per cent above the TUMBLER composite curve at the 10 psi. level and the difference diminishes at both higher and lower overpressures. The two curves intersect at about 270 psi. No significance is attached to this agreement at very high overpressures, since there is no a priori reason for expecting the purely empirical formula (3.1) to be applicable so far beyond the range of overpressures for which it was derived, but the convergence of the two curves in the range of overpressures between those covered by the Naval Ordnance Laboratory data and the present results indicates very satisfactory consistency between the two sets of data.

4.2 RECOMMENDATIONS

It is considered that the present results confirm the practical validity of the Fuchs scaling law for altitude effects, but the extrapolation of the normalized free air peak overpressure curve to low overpressure may still be questionable because of the necessity of using an assumed reflection factor in the reduction of the data. This extrapolation is particularly important in connection with the calculation of blast effects on aircraft. It is therefore recommended that similar blast pressure measurements be made with parachute-borne gages distributed about an atomic bomb fired at a sufficient altitude to give a clear separation of the direct and reflected shocks over a large range of distances. At the same time it would be desirable to obtain data on the path of the triple point at high altitudes. Since the present tests showed no detectable asymmetry in the pressure pattern because of wind, it is considered that these objectives can be accomplished with two vertical arrays, one placed approximately above the bomb and one offset horizontally in a position to intercept the expected path of the triple point and to measure the blast pressure in and above the Mach stem.

---

[5] Operation TUMBLER, Preliminary Test Data Furnished by Armed Forces Special Weapons Project

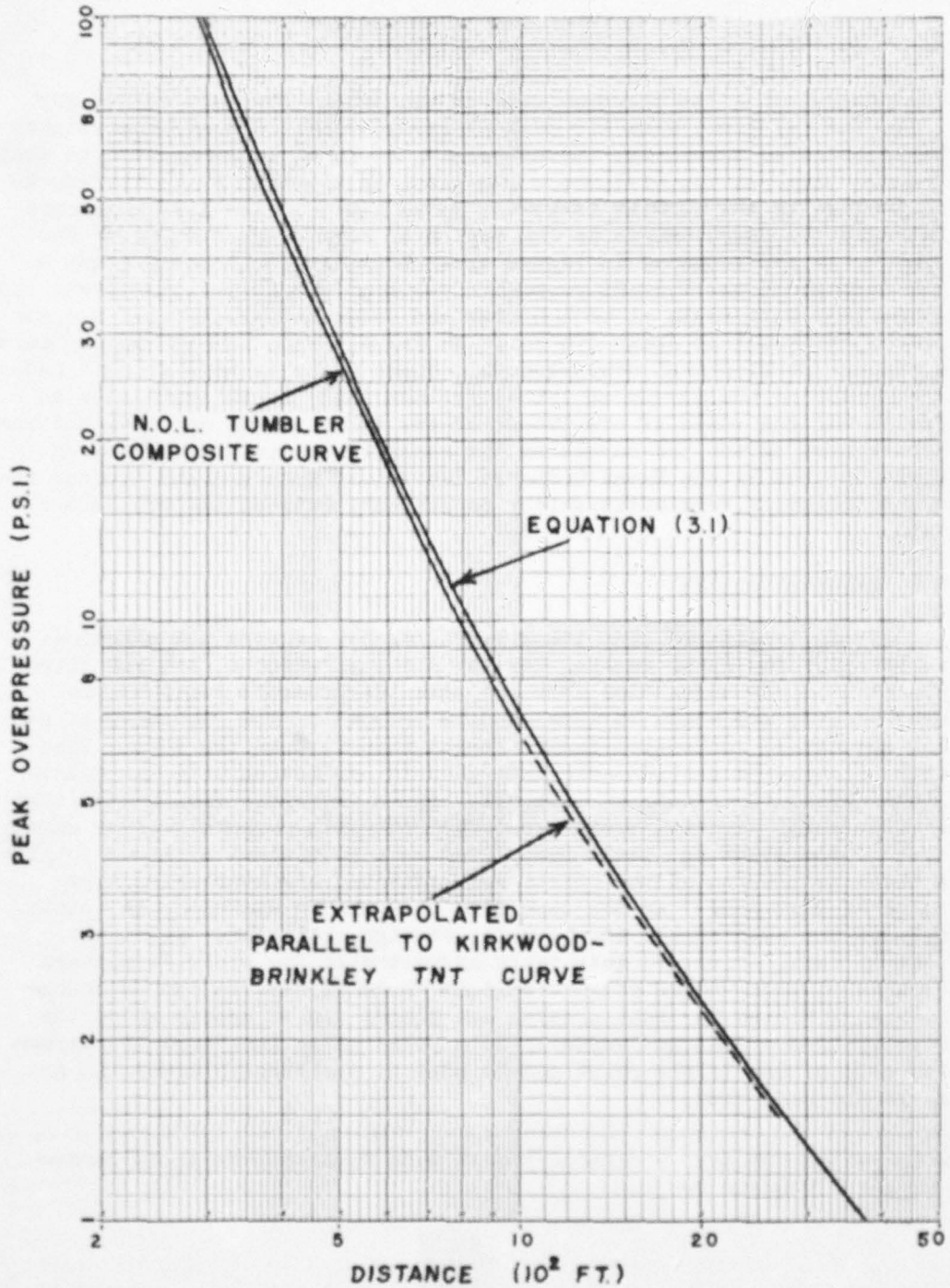

Fig. 4.2 Comparison of Normalized Free Air Peak Overpressure Curves

APPENDIX A

COMPUTATION OF RANGE FROM SHOCK TRAVEL TIME

For the purpose of computing slant ranges from the observed travel times the following procedure was adopted. We first consider an isothermal atmosphere at constant pressure P_o and sound velocity c_o with no wind. The travel time of a shock wave to a radial distance R from the source is

$$t = \int_o^R U^{-1} dr \qquad (A.1)$$

where U is the shock wave velocity given by the Rankine-Hugoniot equation

$$U = c_o \left(1 + \frac{\gamma+1}{2\gamma} \frac{\Delta P}{P_o}\right) \qquad (A.2)$$

$\gamma = 1.4$ for air

ΔP = Peak overpressure

In order to evaluate the integral (A.1) numerically, the dependence of ΔP on R must be known, and this cannot in general be considered as given in advance. However, if we consider only ranges large enough so that $\Delta P/P_o$ is a small quantity over a large part of the path, it is not necessary to know ΔP as a function of R with great precision to obtain fairly accurate values of t as a function of R, and it is sufficient to use the expected rather than the unknown actual value of $\Delta P(R)$ in calculating the integral. It is possible then to compute the average velocity, $V = R/t$, and express it as a function of either R or t. Expressed in this way, V depends on the yield of the source, but if by using the expected values of overpressure as a function of range, V is expressed as a function of ΔP, the result is a relation that is independent of the yield of the source. This is possible because the yield scaling law leaves velocity and pressure unchanged and transforms only distance and time. With a measured value of t and ΔP from a given gage, it is possible to determine the value of V corresponding to the observed ΔP, and with this information the range corresponding to the observed value of t can be computed without any prior knowledge of the yield of the source.

To go from the hypothetical homogeneous isothermal atmosphere to the conditions of the actual atmosphere, use is made of a simplified scaling law, which Bond has shown to be approximately equivalent to

the more complex Fuchs scaling law.[6] This consists essentially of using the Sachs scale factor computed for the altitude of the pressure gage rather than the altitude of the source. According to this law overpressure is changed in the same ratio as ambient pressure, so that $\Delta P/P_o$ is unchanged, and the shock velocity is changed in the same ratio as the velocity of sound. Thus if $\bar{c}$ is an average value of the sound velocity over the path from source to gage, the ratio $U/\bar{c}$, when expressed as a function of $\Delta P/P_o$ is approximately independent of the ambient pressure and temperature at either source or gage as well as the yield of the source. This function, when computed from the expected overpressure vs. distance curve for 1 KT in a homogeneous atmosphere, is then directly applicable to any yield in any atmosphere. Values of this function obtained by numerical integration using the overpressure vs. distance function given by equations (3.1) and (3.2), are plotted in Figure A.1. In using this relation to determine the average shock velocity for a given value of the ratio $\Delta P/P_o$, the way in which the average sound velocity, $\bar{c}$, is defined is not particularly critical for moderate accuracy requirements since c varies by only 14 to 15 per cent between sea level and the tropopause. For the present purpose, c is taken to be

$$\bar{c}(z) = (z-h) \Big/ \int_h^z c^{-1}(z)\, dz \qquad (A.3)$$

where z is the altitude of the gage and h is that of the bomb. This function was computed from the meteorological data for each shot by numerical integration.

The effect of wind velocity was taken into consideration by adding to the average shock velocity the average component of wind velocity projected on the line from shot to gage. Since the wind component represents only a relatively small correction in the average shock velocity, the way in which the average is defined is not critical. In the present case the average is defined by weighting the wind velocity in each small increment in altitude in proportion to the time that would be taken for a sound wave to pass through the given range of altitude.

As mentioned in Chapter 3 of the present report, the ranges computed from the observed travel times, altitudes, and overpressure by the above procedure are found to average about 2.2 per cent larger than the MDTS ranges. While the accuracy of the basic data is not sufficient to warrant a detailed analysis of the source of this small sys-

---

6/ J. W. Bond, Jr., Scaling of Peak Overpressure in a Non-uniform Atmosphere, SC-1939 (Tr), Sandia Corporation, 1 July 1951.

tematic error, it is worth pointing out that its sign is consistent with the TUMBLER free air peak overpressure curve. The TUMBLER curve falls slightly below the curve used in the present computations, and our computed ranges should therefore be slightly too large.

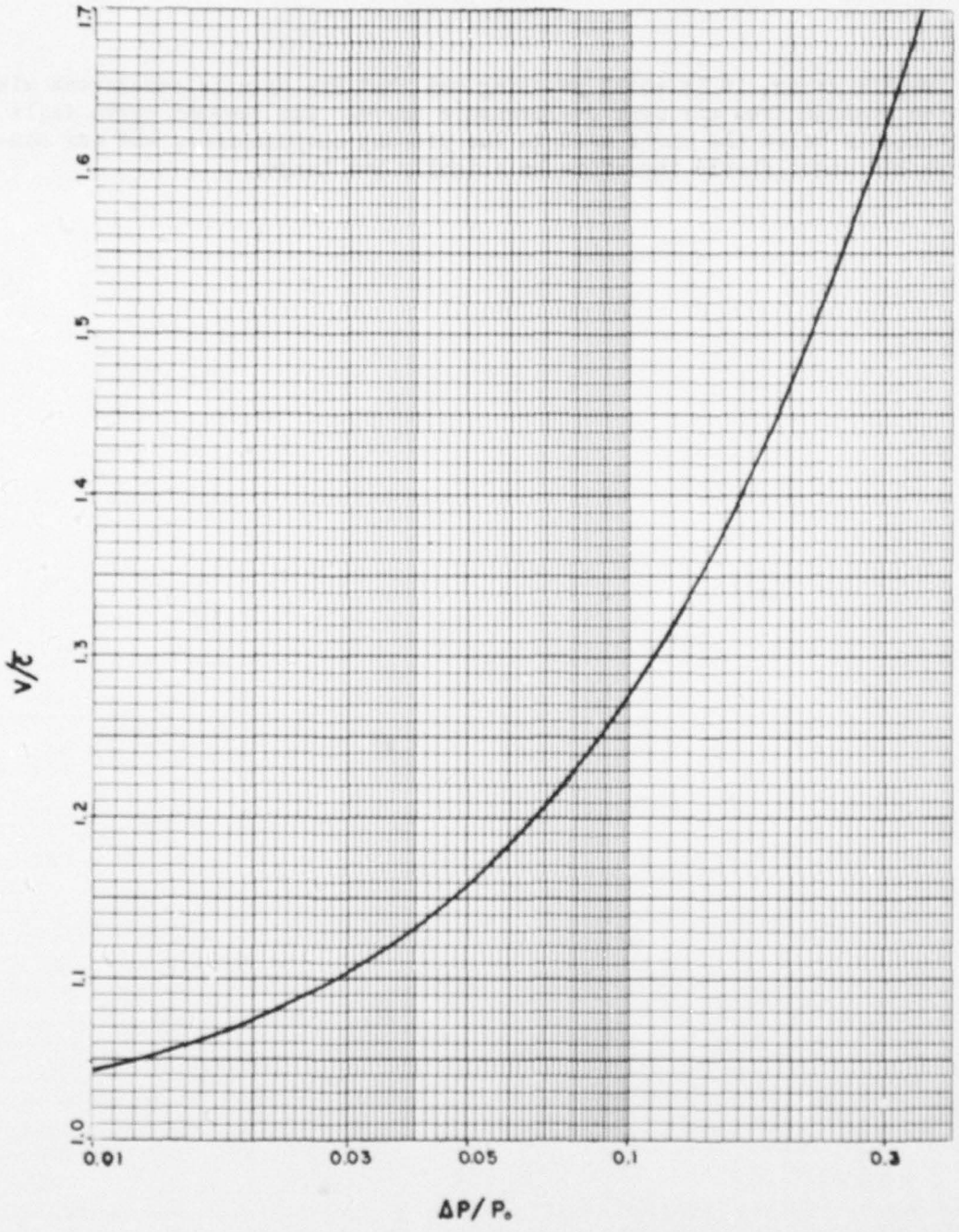

Fig. A.1 Ratio of Average Shock Velocity to Average Sound Velocity ($\bar{V}/\bar{c}$) as a Function of the Ratio of Overpressure to Ambient Pressure ($\Delta P/P_o$)

APPENDIX B

METEOROLOGICAL DATA

TABLE B.1

Shot 5 Radiosonde Data for 7 May 1952, 1200Z (=0500 PDT)

True Altitude (ft. above MSL)	Pressure (psi)	Temperature (°C)	Sound Velocity (ft/sec)	Wind Velocity (ft/sec)	Wind Direction
4127	12.78	18	1122	0	-
5000	12.28	18	1122	0	-
6000	11.87	17	1120	34	180
7000	11.42	14	1115	44	180
8000	11.01	12	1111	54	180
9000	10.59	9	1105	59	190
10,000	10.19	6	1099	61	180
12,000	9.48	1	1090	76	190
14,000	8.76	-4	1079	91	190
15,000	8.43	-7	1074	83	190
16,000	8.11	-9	1070	81	210
18,000	7.50	-14	1059	98	210
20,000	6.92	-16	1055	113	220
22,000	6.37	-21	1045	125	220
24,000	5.85	-27	1033	128	220
25,000	5.60	-30	1026	132	220
26,000	5.37	-32	1022	133	220
28,000	4.93	-36	1013	160	220
30,000	4.50	-41	1002	157	220

TABLE B.2

Shot 8 Radiosonde Data for 5 June 1952, 1200Z (≈0500 PDT)

True Altitude (ft. above MSL)	Pressure (psi)	Temperature (°C)	Sound Velocity (ft/sec)	Wind Velocity (ft/sec)	Wind Direction
4127	12.68	15	1117	5	340
5000	12.29	18	1122	3	340
6000	11.88	16	1118	3	270
7000	11.46	14	1115	8	180
8000	11.06	12	1111	17	130
9000	10.68	10	1107	27	140
10,000	10.29	8	1103	29	130
12,000	9.56	3	1093	32	130
14,000	8.85	-1	1086	34	120
15,000	8.50	-4	1079	34	130
16,000	8.17	-6	1076	29	140
18,000	7.56	-9	1070	24	150
20,000	6.98	-10	1067	32	160
22,000	6.44	-14	1059	35	170
24,000	5.93	-19	1049	42	190
25,000	5.67	-22	1043	42	180
26,000	5.47	-24	1039	44	160
28,000	5.03	-29	1028	39	170
30,000	4.61	-34	1017	32	180
35,000	3.71	-44	996	76	210
40,000	2.92	-53	976	79	200
43,000	2.54	-57	967	74	200

APPENDIX C

ALTITUDE SCALE FACTORS

TABLE C.1

Shot 5

Altitude (kft. above M.S.L.)	λ	μ	Altitude (kft. above M.S.L.)	λ	μ
4.5	1.000	1.000	19.5	1.487	1.151
5.5	1.021	1.002	20.5	1.533	1.166
6.5	1.043	1.007	21.5	1.583	1.180
7.5	1.066	1.012	22.5	1.634	1.197
8.5	1.092	1.020	23.5	1.689	1.214
9.5	1.120	1.029	24.5	1.747	1.233
10.5	1.149	1.038	25.5	1.808	1.249
11.5	1.180	1.050	26.5	1.873	1.274
12.5	1.213	1.062	27.5	1.942	1.295
13.5	1.246	1.073	28.5	2.014	1.318
14.5	1.282	1.084	29.5	2.091	1.340
15.5	1.320	1.097	30.5	2.173	1.362
16.5	1.359	1.111	31.5	2.260	1.386
17.5	1.399	1.124	32.5	2.353	1.411
18.5	1.442	1.138			

ALTITUDE SCALE FACTORS

TABLE C.2

Shot 8

Altitude (kft. above M.S.L.)	λ	μ	Altitude (kft. above M.S.L.)	λ	μ
4.5	1.000	1.000	20.5	1.477	1.121
5.5	1.018	0.999	21.5	1.520	1.132
6.5	1.038	1.003	22.5	1.566	1.145
7.5	1.059	1.008	23.5	1.614	1.160
8.5	1.082	1.014	24.5	1.664	1.173
9.5	1.107	1.020	25.5	1.718	1.190
10.5	1.133	1.027	26.5	1.775	1.209
11.5	1.161	1.037	27.5	1.834	1.226
12.5	1.189	1.043	28.5	1.897	1.243
13.5	1.220	1.051	29.5	1.984	1.276
14.5	1.252	1.059	30.5	2.035	1.284
15.5	1.285	1.068	31.5	2.110	1.306
16.5	1.321	1.079	32.5	2.189	1.328
17.5	1.358	1.090	33.5	2.273	1.352
18.5	1.396	1.100	34.5	2.362	1.375
19.5	1.436	1.109	35.5	2.456	1.401

[redacted]

BIBLIOGRAPHY

N. A. Haskell, J. O. Vann, The Measurement of Free Air Atomic Blast Pressures, Operation JANGLE, Project 1.3c, Air Force Cambridge Research Center

K. Fuchs - Los Alamos Technical Series LA-1021, Vol VII, Pt. II, Chapter 9

R. G. Sachs - The Dependence of Blast on Ambient Temperature and Pressure, Ballistic Research Laboratories, Aberdeen Proving Ground, Report #466 (May 1944)

Operation TUMBLER, Preliminary Test Data Furnished By Armed Forces Special Weapons Project

J. W. Bond, Jr., Scaling of Peak Overpressure in a Non-uniform Atmosphere, SC - 1939 (Tr.), Sandia Corporation, 1 July 1951

[redacted]

DISTRIBUTION

Copy No.

ARMY ACTIVITIES

Asst. Chief of Staff, G-2, D/A, Washington 25, D. C.	1
Asst. Chief of Staff, G-3, D/A, Washington 25, D. C. ATTN: Dep. Asst. CofS, G-3, (RR&SW)	2
Asst. Chief of Staff, G-4, D/A, Washington 25, D. C.	3
Chief of Ordnance, D/A, Washington 25, D. C. ATTN: ORDTX-AR	4
Chief Signal Officer, D/A, P&O Division, Washington 25, D. C. ATTN: SIGOP	5- 7
The Surgeon General, D/A, Washington 25, D. C. ATTN: Chairman, Medical R&D Board	8
Chief Chemical Officer, D/A, Washington 25, D. C.	9- 10
Chief of Engineers, D/A, Military Construction Division, Protective Construction Branch, Washington 25, D. C. ATTN: ENGEB	11
Chief of Engineers, D/A, Civil Works Division, Washington 25, D. C. ATTN: Engineering Division, Structural Branch	12
The Quartermaster General, CBR, Liaison Office, Research and Development Division, D/A, Washington 25, D. C.	13
Office, Chief of Transportation, D/A, Washington 25, D. C. ATTN: Military Planning and Intelligence	14
Chief, Army Field Forces, Ft. Monroe, Va.	15- 17
Army Field Forces Board #1, Ft. Bragg, N. C.	18
Army Field Forces Board #2, Ft. Knox, Ky.	19
Army Field Forces Board #4, Ft. Bliss, Tex.	20
Commanding General, First Army, Governor's Island, New York 4, N. Y. ATTN: G-4, ACofS	21- 23
Commanding General, Second Army, Ft. George G. Meade, Md. ATTN: AIABB	24
Commanding General, Second Army, Ft. George G. Meade, Md. ATTN: AIAME	25
Commanding General, Second Army, Ft. George G. Meade, Md. ATTN: AIACM	26
Commanding General, Third Army, Ft. McPherson, Ga. ATTN: ACofS, G-3	27- 28
Commanding General, Fourth Army, Ft. Sam Houston, Tex. ATTN: G-3 Section	29- 30
Commanding General, Fifth Army, 1660 Hyde Park Blvd., Chicago 15, Ill. ATTN: ALFEN	31
Commanding General, Fifth Army, 1660 Hyde Park Blvd., Chicago 15, Ill. ATTN: ALFOR	32
Commanding General, Fifth Army, 1660 Hyde Park Blvd., Chicago 15, Ill. ATTN: ALFMD-O	33- 36

DISTRIBUTION (Continued)

	Copy No.
Commanding General, Sixth Army, Presidio of San Francisco, Calif. ATTN: AMGCT-4	37
Commander-in-Chief, European Command, APO 403, c/o PM, New York, N. Y.	38
Commander-in-Chief, U. S. Army Europe, APO 403, c/o PM, New York, N. Y. ATTN: OPOT Division, Com. Dev. Branch	39- 40
Commander-in-Chief, Far East Command, APO 500, c/o PM, San Francisco, Calif. ATTN: ACofS, G-3	41- 45
Commanding General, U. S. Army Alaska, APO 942, c/o PM, Seattle, Wash.	46
Commanding General, U. S. Army Caribbean, APO 834, c/o PM, New Orleans, La. ATTN: CG, USARCARIB	47
Commanding General, U. S. Army Caribbean, APO 834, c/o PM, New Orleans, La. ATTN: CG, USARFANT	48
Commanding General, U. S. Army Caribbean, APO 834, c/o PM, New Orleans, La. ATTN: Cml. Off., USARCARIB	49
Commanding General, U. S. Army Caribbean, APO 834, c/o PM, New Orleans, La. ATTN: Surgeon, USARCARIB	50
Commanding General, USAR Pacific, APO 958, c/o PM, San Francisco, Calif. ATTN: Cml. Off.	51- 52
Commanding General, Trieste U. S. Troops, APO 209, c/o PM, New York, N. Y. ATTN: ACofS, G-3	53
Commandant, Command and General Staff College, Ft. Leavenworth, Kan. ATTN: ALLIS(AS)	54- 55
Commandant, The Infantry School, Ft. Benning, Ga. ATTN: C.D.S.	56- 57
Commandant, The Artillery School, Ft. Sill, Okla.	58
Commandant, The AA&GM Branch, The Artillery School, Ft. Bliss, Tex.	59
Commandant, The Armored School, Ft. Knox, Ky. ATTN: Classified Document Section, Evaluation and Res. Division	60- 61
Commanding General, Medical Field Service School, Brooke Army Medical Center, Ft. Sam Houston, Tex.	62
Commandant, Army Medical Service School, Walter Reed Army Medical Center, Washington 25, D. C. ATTN: Dept. of Biophysics	63
The Superintendent, United States Military Academy, West Point, N. Y. ATTN: Professor of Ordnance	64- 65
Commanding General, The Transportation Corps Center and Ft. Eustis, Ft. Eustis, Va. ATTN: Asst. Commandant, Military Sciences and Tactics	66
Commandant, Chemical Corps School, Chemical Corps Training Command, Ft. McClellan, Ala.	67
Commanding General, Research and Engineering Command, Army Chemical Center, Md. ATTN: Special Projects Officer	68
RD Control Officer, Aberdeen Proving Ground, Md. ATTN: Director, Ballistics Research Laboratory	69- 70

DISTRIBUTION (Continued)

	Copy No.
Commanding General, The Engineer Center, Ft. Belvoir, Va. ATTN: Asst. Commandant, The Engineer School	71- 73
Chief of Research and Development, D/A, Washington 25, D. C.	74
Commanding Officer, Engineer Research and Development Laboratory, Ft. Belvoir, Va. ATTN: Chief, Technical Intelligence Branch	75
Commanding Officer, Picatinny Arsenal, Dover, N. J. ATTN: ORDBB-TK	76
Commanding Officer, Army Medical Research Laboratory, Ft. Knox, Ky.	77
Commanding Officer, Chemical Corps Chemical and Radiological Laboratory, Army Chemical Center, Md. ATTN: Technical Library	78- 79
Commanding Officer, Transportation R&D Station, Ft. Eustis, Va.	80
Commanding Officer, Psychological Warfare Center, Ft. Bragg, N. C. ATTN: Library	81
Asst. Chief, Military Plans Division, Rm 516, Bldg. 7, Army Map Services, 6500 Brooks Lane, Washington 25, D. C. ATTN: Operations Plans Branch	82
Director, Technical Documents Center, Evans Signal Laboratory, Belmar, N. J.	83
Director, Waterways Experiment Station, PO Box 631, Vicksburg, Miss. ATTN: Library	84
Director, Operations Research Office, Johns Hopkins University, 6410 Connecticut Ave., Chevy Chase, Md. ATTN: Library	85

NAVY ACTIVITIES

Chief of Naval Operations, D/N, Washington 25, D. C. ATTN: OP-36	86- 87
Chief of Naval Operations, D/N, Washington 25, D. C. ATTN: OP-51	88
Chief of Naval Operations, D/N, Washington 25, D. C. ATTN: OP-53	89
Chief of Naval Operations, D/N, Washington 25, D. C. ATTN: OP-374 (OEG)	90
Chief, Bureau of Medicine and Surgery, D/N, Washington 25, D. C. ATTN: Special Weapons Defense Division	91- 92
Chief, Bureau of Ordnance, D/N, Washington 25, D. C.	93
Chief, Bureau of Personnel, D/N, Washington 25, D. C. ATTN: Pers 15	94
Chief, Bureau of Personnel, D/N, Washington 25, D. C. ATTN: Pers C	95
Chief, Bureau of Ships, D/N, Washington 25, D. C. ATTN: Code 348	96

[redacted]

DISTRIBUTION (Continued)

	Copy No.
Chief, Bureau of Supplies and Accounts, D/N, Washington 25, D. C.	97
Chief, Bureau of Yards and Docks, D/N, Washington 25, D. C. ATTN: P-312	98
Chief, Bureau of Aeronautics, D/N, Washington 25, D. C.	99-100
Office of Naval Research, Code 219, Rm 1807, Bldg. T-3, Washington 25, D. C. ATTN: RD Control Officer	101
Commander-in-Chief, U. S. Atlantic Fleet, Fleet Post Office, New York, N. Y.	102-103
Commander-in-Chief, U. S. Pacific Fleet, Fleet Post Office, San Francisco, Calif.	104-105
Commander, Operation Development Force, U. S. Atlantic Fleet, U. S. Naval Base, Norfolk 11, Va. ATTN: Tactical Development Group	106
Commander, Operation Development Force, U. S. Atlantic Fleet, U. S. Naval Base, Norfolk 11, Va. ATTN: Air Department	107
Commandant, U. S. Marine Corps, Headquarters, USMC, Washington 25, D. C. ATTN: (A03H)	108-111
President, U. S. Naval War College, Newport, Rhode Island	112
Superintendent, U. S. Naval Postgraduate School, Monterey, Calif.	113
Commanding Officer, U. S. Naval Schools Command, Naval Station, Treasure Island, San Francisco, Calif.	114-115
Director, USMC Development Center, USMC Schools, Quantico, Va. ATTN: Marine Corps Tactics Board	116
Director, USMC Development Center, USMC Schools, Quantico, Va. ATTN: Marine Corps Equipment Board	117
Commanding Officer, Fleet Training Center, Naval Base, Norfolk 11, Va. ATTN: Special Weapons School	118-119
Commanding Officer, Fleet Training Center, (SPWP School), Naval Station, San Diego 36, Calif.	120-121
Commander, Air Force, U. S. Pacific Fleet, Naval Air Station, San Diego, Calif.	122
Commander, Training Command, U. S. Pacific Fleet, c/o Fleet Sonar School, San Diego 47, Calif.	123
Commanding Officer, Air Development Squadron 5, USN Air Station, Moffett Field, Calif.	124
Commanding Officer, Naval Damage Control Training Center, U. S. Naval Base, Philadelphia 12, Pa. ATTN: ABC Defense Course	125
Commanding Officer, Naval Unit, Chemical Corps School, Ft. McClellan, Ala.	126
Joint Landing Force Board, Marine Barracks, Camp Lejeune, N. C.	127

[redacted] [redacted]

DISTRIBUTION (Continued) Copy No.

Commander, U. S. Naval Ordnance Laboratory, Silver Spring 19, Md. ATTN: EE 128
Commander, U. S. Naval Ordnance Laboratory, Silver Spring 19, Md. ATTN: Alias 129
Commander, U. S. Naval Ordnance Laboratory, Silver Spring 19, Md. ATTN: Aliex 130
Commander, U. S. Naval Ordnance Test Station, Inyokern, China Lake, Calif. 131
Officer-in-Charge, U. S. Naval Civil Engineering Research and Evaluation Laboratory, Construction Battalion Center, Port Hueneme, Calif. ATTN: Code 753 132-133
Commanding Officer, USN Medical Research Institute, National Naval Medical Center, Bethesda 14, Md. 134
Director, U. S. Naval Research Lboratory, Washington 25, D. C. 135
Commanding Officer and Director, USN Electronics Laboratory, San Diego 52, Calif. ATTN: Code 210 136
Commanding Officer, USN Radiological Defense Laboratory, San Francisco, Calif. ATTN: Technical Information Division 137-138
Commanding Officer and Director, David W. Taylor Model Basin, Washington 7, D. C. ATTN: Library 139
Commander, Naval Air Development Center, Johnsville, Pa. 140
Commanding Officer, Office of Naval Research Branch Office, 1000 Geary St., San Francisco, Calif. 141-142

AIR FORCE ACTIVITIES

Surplus in TISOR 143
Asst. for Atomic Energy, Headquarters, USAF, Washington 25, D. C. ATTN: DCS/O 144
Asst. for Development Planning, Headquarters, USAF, Washington 25, D. C. 145-146
Director of Operations, Headquarters, USAF, Washington 25, D. C. 147-148
Director of Plans, Headquarters, USAF, Washington 25, D. C. ATTN: War Plans Division 149
Directorate of Requirements, Headquarters, USAF, Washington 25, D. C. ATTN: AFDRQ-SA/M 150
Directorate of Research and Development, Armament Division, DCS/D, Headquarters, USAF, Washington 25, D. C. 151
Directorate of Intelligence, Headquarters, USAF, Washington 25, D. C. 152-153
The Surgeon General, Headquarters, USAF, Washington 25, D. C. 154-155

DISTRIBUTION (Continued)

	Copy No.
Commanding General, U. S. Air Forces Europe, APO 633, c/o PM, New York, N. Y.	156
Commanding General, Far East Air Forces, APO 925, c/o PM, San Francisco, Calif.	157
Commanding General, Alaskan Air Command, APO 942, c/o PM, Seattle, Wash. ATTN: AAOTN	158-159
Commanding General, Northeast Air Command, APO 862, c/o PM, New York, N. Y.	160
Commanding General, Strategic Air Command, Offutt AFB, Omaha, Neb. ATTN: Chief, Operations Analysis	161
Commanding General, Tactical Air Command, Langley AFB, Va. ATTN: Documents Security Branch	162-164
Commanding General, Air Defense Command, Ent AFB, Colo.	165-166
Commanding General, Air Materiel Command, Wright-Patterson AFB, Dayton, Ohio	167-169
Commanding General, Air Training Command, Scott AFB, Belleville, Ill.	170-171
Commanding General, Air Research and Development Command, PO Box 1395, Baltimore 3, Md. ATTN: RDDN	172-174
Commanding General, Air Proving Ground Command, Eglin AFB, Fla., ATTN: AG/TRB	175
Commanding General, Air University, Maxwell AFB, Ala.	176-180
Commandant, Air Command and Staff School, Maxwell AFB, Ala.	181-182
Commandant, Air Force School of Aviation Medicine, Randolph AFB, Tex.	183-184
Commanding General, Wright Air Development Center, Wright-Patterson AFB, Dayton, Ohio. ATTN: WCOESP	185-190
Commanding General, Air Force Cambridge Research Center, 230 Albany St., Cambridge 39, Mass. ATTN: Atomic Warfare Directorate	191
Commanding General, Air Force Cambridge Research Center, 230 Albany St., Cambridge 39, Mass. ATTN: CRTSL-2	192
Commanding General, AF Special Weapons Center, Kirtland AFB, N. Mex. ATTN: Chief, Technical Library Branch	193-195
Commandant, USAF Institute of Technology, Wright-Patterson AFB, Dayton, Ohio. ATTN: Resident College	196
Commanding General, Lowry AFB, Denver, Colo. ATTN: Dept. of Armament Training	197-198
Commanding General, 1009th Special Weapons Squadron, Tempo "T", 14th & Constitution Sts., NW, Washington 25, D.C.	199-201
The RAND Corporation, 1700 Main St., Santa Monica, Calif. ATTN: Nuclear Energy Division	202-203

OTHER DEPT. OF DEFENSE ACTIVITIES

Executive Secretary, Joint Chiefs of Staff, Washington 25, D. C. ATTN: Joint Strategic Plans Committee	204

DISTRIBUTION (Continued) Copy No.

Director, Weapons Systems Evaluation Group, OSD, Rm 2E1006, Pentagon, Washington 25, D. C. 205
Asst. for Civil Defense, OSD, Washington 25, D. C. 206
Chairman, Armed Services Explosives Safety Board, D/D, Rm 2403, Barton Hall, Washington 25, D. C. 207
Chairman, Research and Development Board, D/D, Washington 25, D. C. ATTN: Technical Library 208
Executive Secretary, Committee on Atomic Energy, Research and Development Board, Rm 3E1075, Pentagon, Washington 25, D. C. 209-210
Executive Secretary, Military Liaison Committee, PO Box 1814, Washington 25, D. C. 211
Commandant, National War College, Washington 25, D. C. ATTN: Classified Records Section, Library 212
Commandant, Armed Forces Staff College, Norfolk 11, Va. ATTN: Secretary 213
Commanding General, Field Command, AFSWP, PO Box 5100, Albuquerque, N. Mex. 214-219
Chief, AFSWP, PO Box 2610, Washington 13, D. C. 220-228

ATOMIC ENERGY COMMISSION ACTIVITIES

University of California Radiation Laboratory, PO Box 808, Livermore, Calif. ATTN: Margaret Folden 229
U. S. Atomic Energy Commission, Classified Document Room, 1901 Constitution Ave., Washington 25, D. C. ATTN: Mrs. J. M. O'Leary (for DMA) 230-232
Los Alamos Scientific Laboratory, Report Library, PO Box 1663, Los Alamos, N. Mex. ATTN: Helen Redman 233-235
Sandia Corporation, Classified Document Division, Sandia Base, Albuquerque, N. Mex. ATTN: Wynne K. Cox 236-255
Weapon Test Reports Group, TIS 256
Surplus in TISOR for AFSWP 257-305

ADDITIONAL DISTRIBUTION

Director of Special Weapons Developments, OCAFF, Fort Bliss, Tex. ATTN: Major Hale Mason, Jr. 306

AEC, Oak Ridge, Penn., AJ1898

[redacted] [redacted]